A NARROWBAND, WIDE DYNAMIC RANGE RECEIVER FOR AMPLITUDE AND PHASE MEASUREMENT OF ELECTROMAGNETIC WAVES

by

William Joseph Schintler

A thesis submitted in partial fulfillment
of the requirements for the Master of
Science degree in Electrical and Computer Engineering
in the Graduate College of
The University of Iowa

December 1990

Thesis supervisor: Professor Norbert R. Malik

Graduate College
The University of Iowa
Iowa City, Iowa

CERTIFICATE OF APPROVAL

MASTER'S THESIS

This is to certify that the Master's thesis of

William Joseph Schintler

has been approved by the Examining Committee for the thesis requirement for the Master of Science degree in Electrical and Computer Engineering at the December 1990 graduation.

Thesis committee: N R Mahle
Thesis supervisor

John P. Robinson
Member

David A. Barnett
Member

ACKNOWLEDGMENTS

The author would like to express his sincere appreciation to Professor Norbert R. Malik for supervising this project and assisting with the structure of the thesis.

Dr. Donald Gurnett and Mr. Donald Kirchner, both of the University of Iowa Physics and Astronomy Department, are thanked for their suggestions and advice on various points concerning this project. Mr. Terrance Averkamp and Mr. Charles Herscovici are thanked for providing the necessary software support for the receiver.

Thanks are due to Mrs. Kathy Kurth who completed the final typed copy of this thesis. Ms. Stephanie Kunkle is thanked for efficiently drawing several figures included in this work.

TABLE OF CONTENTS

LIST OF TABLES

LIST OF FIGURES

INTRODUCTION

Background

This thesis is concerned with the design and implementation of a receiver system which is part of a University of Iowa spacecraft instrument designed to investigate properties of electromagnetic and electrostatic waves in the earth's magnetosphere. The objectives of this investigation are to make amplitude measurements of waves over a wide dynamic range and to accurately measure the phase of signals received by pairs of orthogonal antennas mounted on the spacecraft. Both of these measurements are to be accomplished with relatively high frequency resolution.

The waves originate from plasma interactions in a region of ionized gas surrounding the earth called the magnetosphere. The electrostatic and electromagnetic waves produced by these interactions propagate through the magnetosphere to the spacecraft. Here, they are converted to electrical signals which are processed by the instrument.

The instrument, which is a subsystem of the POLAR satellite, has several objectives. It will measure spectral and wave vector characteristics of electromagnetic and electrostatic waves over a wide frequency range. The spectrum and wave vector characteristics of waves generated by ground-based active experiments will also be

measured. Finally, the measurements will be analyzed and interpreted in collaboration with investigators using other POLAR instruments to study plasma phenomena in the Earth's magnetosphere.

A major purpose of the experiment is the determination of the wave normal, polarization, and Poynting vectors. As discussed by Calvert (see Reference 1), it is possible on a spinning spacecraft to determine the direction of arrival of a wave by measuring the relative phase of signals received by a pair of orthogonal electric antennas. Additionally, the strengths of the fields must be measured as a function of frequency over both a wide dynamic range and a wide frequency range.

Motivation for Specifications

Figure 1 is a diagram of the entire instrument. Three orthogonal electric antennas, three orthogonal magnetic antennas, and a loop antenna, along with their associated preamplifiers, serve as the sensors. The sensors are mounted so as to minimize electromagnetic interference from the spacecraft. A field effect transistor selector switch determines which signals are chosen for analysis by the sweep frequency receiver. Generally, one of the seven antennas is selected for observation by the "A" band and another is selected for the "B" band. Following processing by the receiver, the amplitude information from bands A and B, as well as the phase between the selected antennas, is sent to an 8085 microprocessor based data control unit, where the signals are

Figure 1. General diagram illustrating sweep frequency receiver and related subsystems.

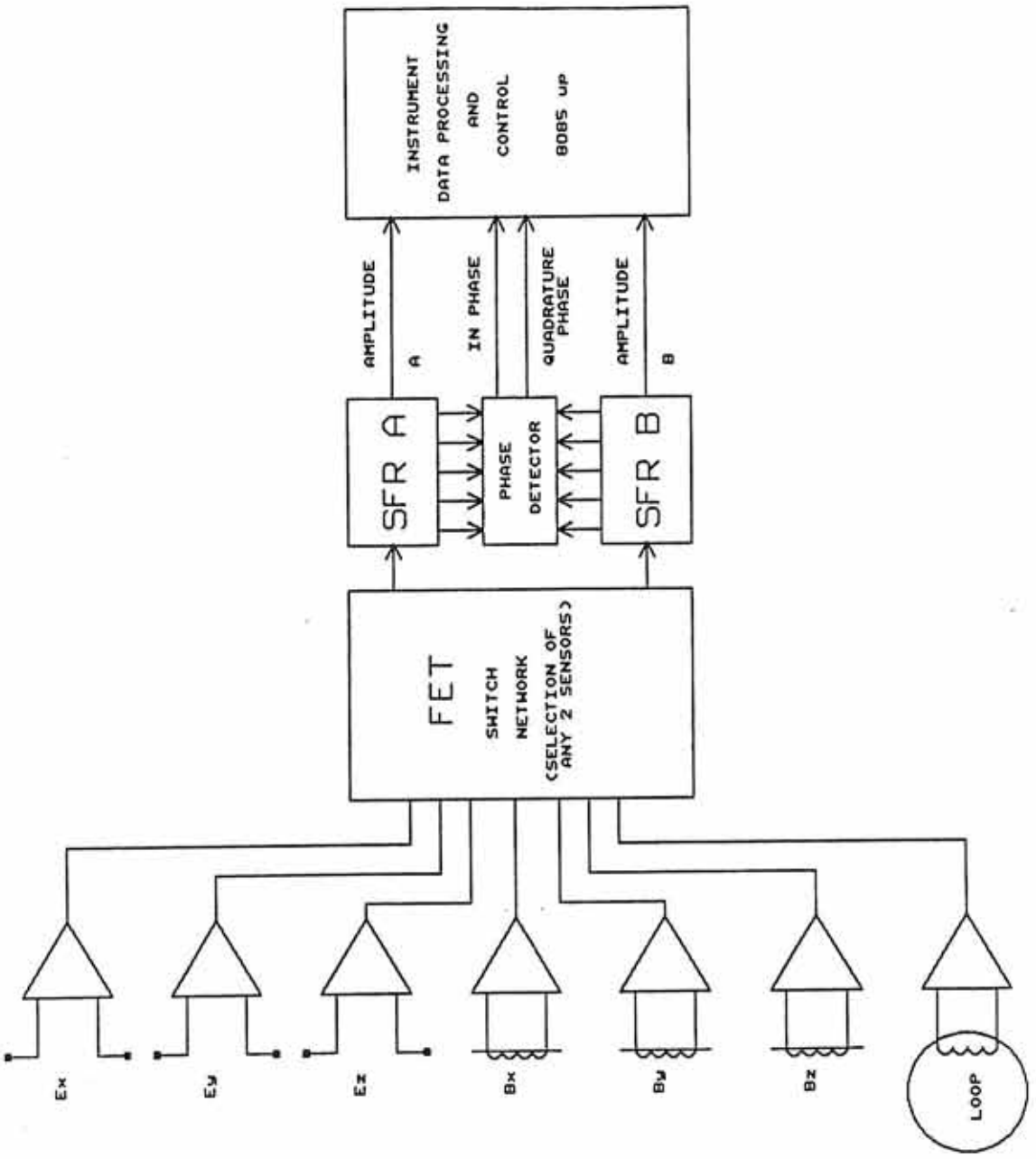
INSTRUMENT
DATA PROCESSING
AND
CONTROL
8085 uP
AMPLITUDE
A
IN PHASE
QUADRATURE
PHASE
AMPLITUDE
B
SFR A
PHASE
DETECTOR
SFR B
FET
SWITCH
NETWORK
(SELECTION OF
ANY 2 SENSORS)
Ex
Ey
Ez
Bx
By
Bz
LOOP

converted to a format suitable for transmission via the spacecraft data system. With this antenna setup, it is possible to observe electromagnetic waves over both a very wide dynamic range and frequency range. There are generally strong emissions at some frequencies and weak emissions at others. Some of the strong electromagnetic plasma wave emissions include Auroral Kilometric Radiation, broadband electrostatic noise and auroral hiss. Auroral Kilometric radiation typically occurs between 30 kHz and 800 kHz and has a bandwidth of 100 kHz. When analyzed with high frequency resolution, this radiation is found to consist of a large number of discrete spectral components. Broadband Electrostatic Noise occurs over a broad range of frequencies between 5 Hz and 10 kHz. Finally, Auroral Hiss spans a frequency range of .1 Hz to 100 kHz and has a bandwidth of 15 kHz.

At the low end of the dynamic range, the sensitivity must be adequate to permit detection of weak emissions such as z-mode and continuum radiation. The dynamic range between the strongest and the weakest of these signals is 100 dB. This sets the desired dynamic range of the receiver.

As is evident from the discussion of strong emissions, the frequency interval of interest ranges from below 30 Hz to as high as 800 kHz. It is desirable that the receiver be able to span this range. Also, due to the fact that many wave intensities follow a roughly 1/f spectral density distribution, the detection bandwidth of

the receiver divided by the frequency of observation (delta f/f) shall be roughly constant over the full frequency range of the receiver. The conflicting demands of fast time response, good phase accuracy, and high frequency resolution are such that the best compromise for delta f/f is about one percent.

One of the primary functions of this receiver is the measurement of phase between two of the seven antennas. It is desirable to measure the phase between sensors to within one degree. On previous receivers of this type, phase measurements have been accomplished at the expense of a major amount of ground software complexity. The phase response varied significantly with changing temperatures and signal levels. With a knowledge of the instrument temperature and signal level, it was possible to subtract the phase offset between the receiver outputs from the measured phase and correct for it. The instruments contained a thermistor so the approximate temperature was known, and each receiver has an amplitude output, so amplitude was known. With the use of a fundamentally different approach in the new receiver design, the phase offset problem is greatly reduced on POLAR.

Although the primary objective of the receiver is frequency domain measurement, it is important that the receiver responds sufficiently quickly to analyze rapidly changing signals. This requirement is true for both the DC outputs corresponding to the logarithm of the observed signal, and the phase outputs. As will be

discussed later, the phase correlators must integrate over several cycles in order to make a good phase measurement. In regard to receiver response time, the design goal will be to make the response as fast as possible but not so fast as to sacrifice accuracy of amplitude and phase measurements.

Two other important receiver considerations are the ability to operate over a wide temperature range and to consume a minimum of power. The instrument baseplate temperature in vacuum is specified to be in the range from -20C to +50C. The receiver electronics is designed to operate from -40C to +70C. The power allocation is two watts. These design goals, and the time response mentioned above, are secondary in importance to frequency response, dynamic range, and phase measurement capabilities.

Proposed Receiver Topology

Figure 2 shows the division of the receiver into channels and frequencies. There are five three octave wide spaced channels, designated by the first number of the label in the box following the word SFR. Each channel consists of two similar subchannels denoted by the A or B in the label. For instance, SFR 5A denotes the "A" band of the top SFR channel. The operating frequency range for this channel spans from 100 kHz to 800 kHz. Figure 3 shows a proposed general receiver block diagram. The circuit shown here is repeated for each of the frequency ranges shown in Figure 2. This allows for each of the five individual receivers to be optimized for operation

Figure 2. Representation of sweep frequency receiver showing channel division and frequencies of operation.

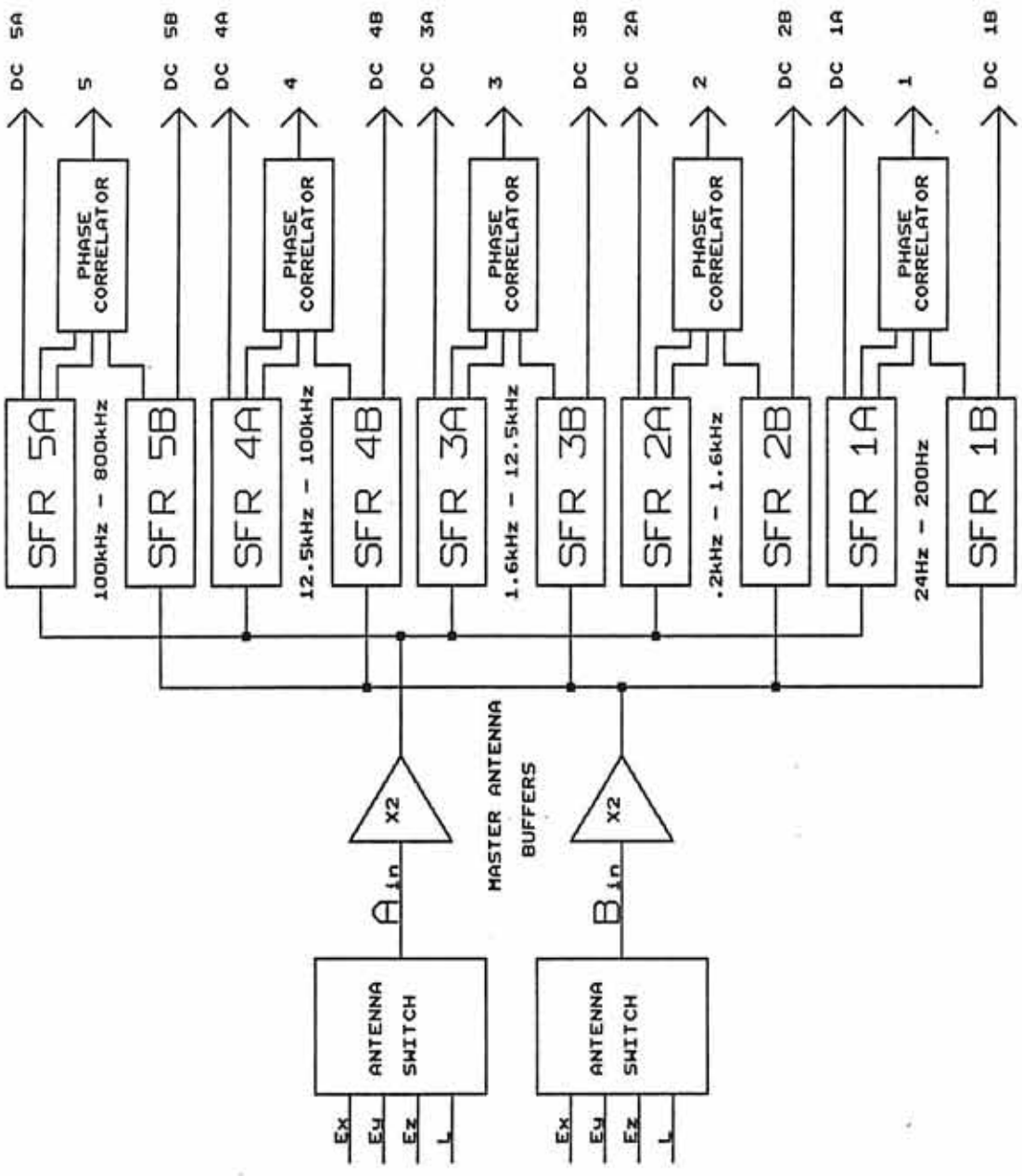
DC 5A
5
DC 5B
DC 4A
4
DC 4B
DC 3A
3
DC 3B
DC 2A
2
DC 2B
DC 1A
1
DC 1B
PHASE CORRELATOR
SFR 5A
100kHz - 800kHz
SFR 5B
SFR 4A
12.5kHz - 100kHz
SFR 4B
SFR 3A
1.6kHz - 12.5kHz
SFR 3B
SFR 2A
.2kHz - 1.6kHz
SFR 2B
SFR 1A
24Hz - 200Hz
SFR 1B
X2
X2
A in
B in
MASTER ANTENNA BUFFERS
ANTENNA SWITCH
ANTENNA SWITCH
Ex
Ey
Ez
L
Ex
Ey
Ez
L

Figure 3. SFR block diagram.

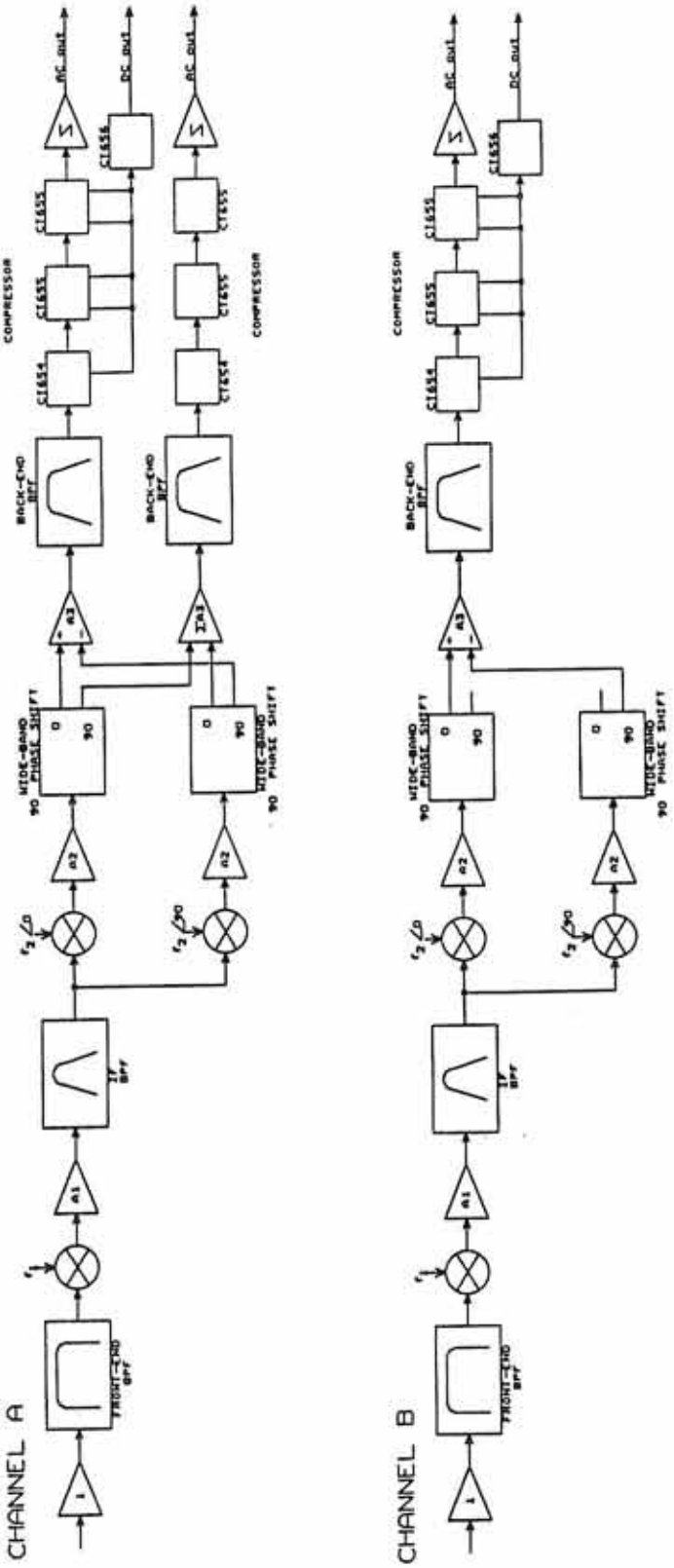
CHANNEL A
CHANNEL B
FRONT-END BPF
1ST BPF
WIDE-BAND 90 PHASE SHIFT
BACK-END BPF
COMPRESSOR
AC_out
DC_out

in its own frequency range with regard to response time and detection bandwidth. The detection bandwidth can be made to approximate the delta f/f rule mentioned above.

There are two important features of this receiver. Referring to Figure 3, the first is that the mixing frequency "f1" continually steps through different frequencies in increasing order. Depending on the mode of operation, there are either 32 or 64 steps; and the spacing of the frequencies is either linear or logarithmic. In general, the different frequency bands step their mixing frequencies at different rates. This allows the lower frequency bands to step slower to compensate for their slower response times. The entire system is referred to as a sweep frequency receiver (SFR).

The other important feature is that this is a single sideband receiver. Figure 4 graphically shows the difference between double sideband detection and single sideband. The need for the single sideband system is easily demonstrated. Looking at Figure 4, one observes that in a double sideband system using down conversion, two distinct regions in frequency space are down converted to the same frequency near baseband. In one of these, represented by FI2 in 4(a), the phase relationships of the original signal are maintained. For the other region, FI1, a phase reversal takes place because it is actually the result of a translation to a negative frequency. When observing arbitrary signals with the receiver, it is impossible to know if it corresponds to FI1 or FI2 and so the phase change is

Figure 4. Graphical representations of downward conversion methods. (a) Graphical representation of double sideband downward conversion. (b) Circuit for single sideband conversion. (c) Graphical representation of single sideband downward conversion.

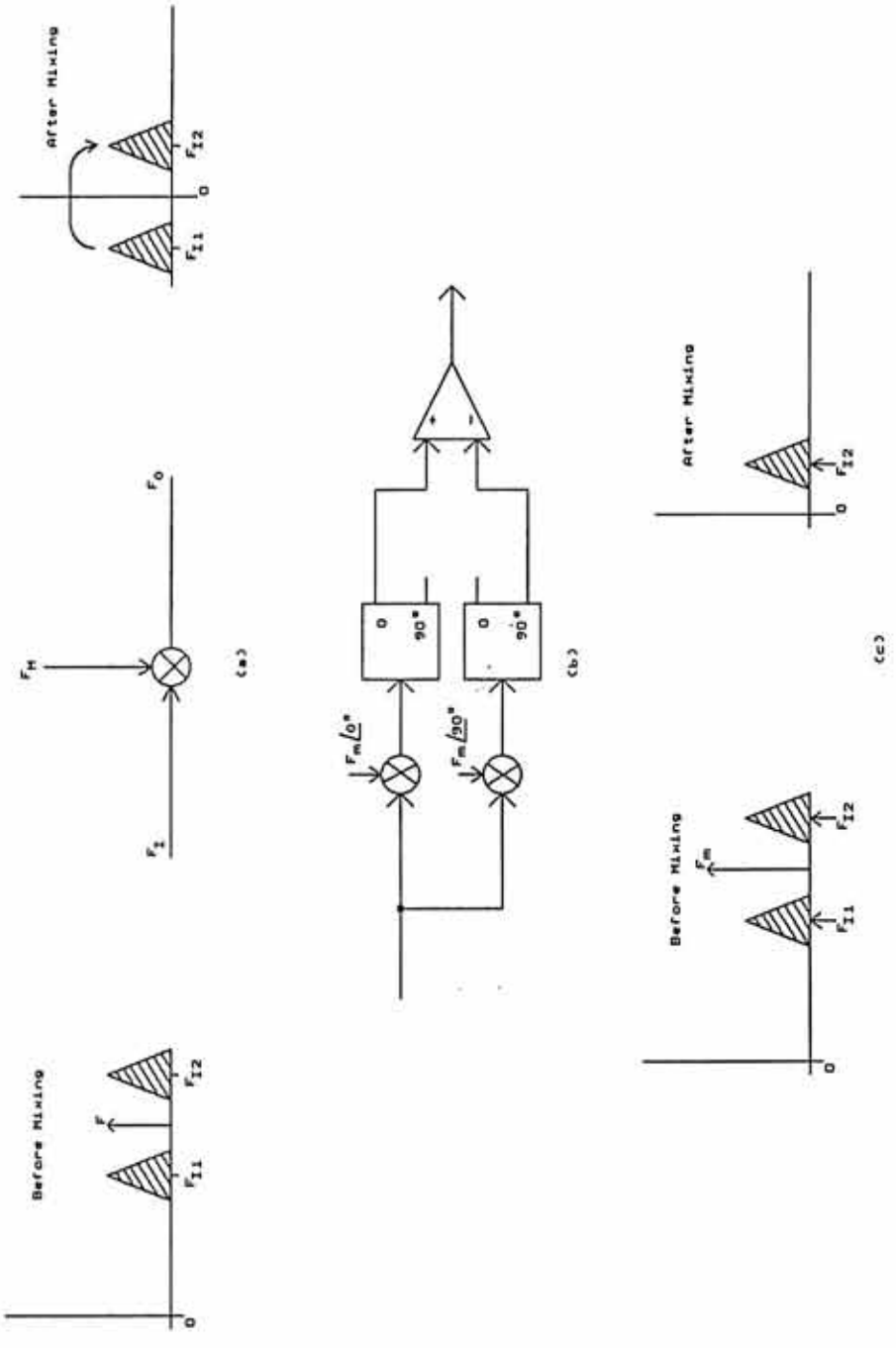
After Mixing
F_{I2}
0
F_{I1}
F_H
F_0
F_1
(a)
0
90°
0
90°
+
-
$F_m/0°$
$F_m/90°$
(b)
After Mixing
F_{I2}
0
Before Mixing
F_m
F_{I2}
F_{I1}
0
(c)
Before Mixing
F
F_{I2}
F_{I1}
0

unknown. This is unacceptable because the receiver must preserve phase, as the output is hard limited and sent to a phase detector to determine the original phase of the antenna signal. For this reason, a single sideband system must be employed as only a single area of frequency space is translated to the receiver output. Appendix 1 derives the method used for the generation.

The possibility of using a very sharp IF filter instead of a single sideband system has been investigated. A receiver prototype with a crystal filter was designed and constructed. The dynamic range and amplitude performance were outstanding. However, the phase changed by more than one thousand degrees over the passband of the filter. The demands placed on the phase matching proved to be unreasonable for this system.

A brief statement of the signal flow in Figure 3 follows. After the buffer at the input, the signal is filtered by the front-end filter whose bandwidth is as wide as the frequency range of a given channel. This is necessary to remove out of band signals which could be mixed to baseband and cause undesired responses. The mixing signal F1 which steps through a range of frequencies converts the antenna signal to a constant intermediate frequency which is handled by an IF filter. Signals F2(0 deg), and F2(90 deg), are two quadrature mixing signals which mix this constant IF frequency down to a low back-end frequency. Through the use of the wide band ninety degree phase shifters and the summing and difference amplifiers, it is possible to

eliminate one sideband of the detected input signal. The back-end filter is about one octave wide and sets the detection bandwidth of the receiver. Each of the series of five amplifiers runs into the summing node of a full-wave diode envelope detector. The result is a DC output which closely approximates a logarithmic amplitude response. The output of the last amplifier is also hard limited and the zero crossings of this waveform contain phase information. The resulting outputs are a DC output, whose value corresponds to the logarithm of the detected signal, and an AC output that retains the phase information of the detected signal.

Proposed Method of Phase Correlation

The compressed AC outputs are instantaneous one bit samples of the waveform which contain only the phase information. This waveform may either be "high" or "low" which corresponds to the logic levels 1 and 0 respectively. As illustrated in Figure 5, the SIN and COS outputs are exclusive OR'ed with the REF outputs. If both inputs to the EX OR are of the same logic level, the output is low. If they are different, the output is high. The two outputs, designated C and S, are simultaneously counted over a time interval of 255 counts. A count is made every time the counter input is high. These counts, designated SINVAL and COSVAL for inputs S and C respectively, are proportional to the percentage of time the EX OR inputs are different in phase. The following manipulations are performed in software by the Instrument Data Processing and Control (see Reference 2).

Figure 5. Exclusive 'OR' circuit for phase correlation.

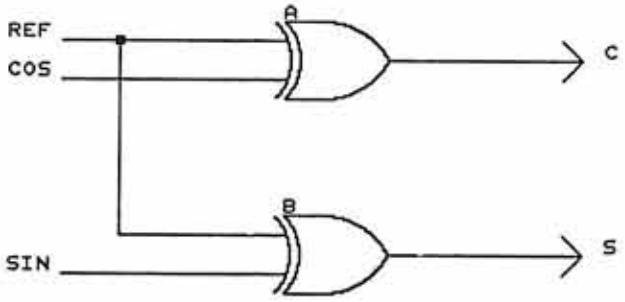
REF
COS
A
C
B
SIN
S

$$S = 180^{0} * (\frac{SinVAL}{255}) - 90^{0} \quad (1)$$

$$C = 180^{0} * (\frac{CosVAL}{255}) - 90^{0} \quad (2)$$

$$PSS = Sin\ (S) \quad (3)$$

$$PSC = -Sin(C) \quad (4)$$

$$\phi = \tan^{-1}\ (PSC/PSS) \quad (5)$$

Equation (5) is the resulting phase angle between the two receiver outputs. As previously mentioned, this angle is proportional to the phase angle between the sensors observed by the receiver.

$$Correlation = \sqrt{PSS^{2} + PSC^{2}} \quad (6)$$

This expression is a measure of the certainty of the measured phase angle in (5). In the ideal correlation, three conditions are necessary for a perfect phase measurement. First, the SIN and COS AC outputs must be in perfect quadrature. Second, the count would be infinite in duration. Finally, the signal to noise ratio of the received signal would be infinite. With these conditions met, the correlation number is unity. It deviates from unity with increasing

uncertainty. When the SIN and COS AC outputs are not in quadrature, it is possible for the correlation to be larger then unity. It is possible for values to range from 0 to 1.4.

DESIGN HERITAGE

Dynamics Explorer

A receiver whose purpose was similar to the Polar SFR was flown on an earlier spacecraft, Dynamics Explorer. A flow diagram of the Dynamics Explorer SFR is shown in Figure 6. It is a double conversion, single sideband receiver like the Polar SFR. The fundamental difference between this design and that on Polar is the way the single sideband detection is derived. Instead of using the previously discussed Hilbert Transform method of single sideband detection, this receiver relies entirely on a sharp intermediate frequency filter to eliminate the lower sideband. This places great demands on the sharpness of the IF filter which results in rapidly changing phase characteristics over the passband. This was the major source of the previously mentioned phase offset.

Two other sources of phase error are the use of another bandpass filter after the compressor to band limit the signal to the operating range of the wideband phase shifters and an RC integrator instead of the counter used in POLAR for phase correlations. The proposed circuit topology for the new receiver largely eliminates these sources of phase error.

In order to describe the performance of the Dynamics Explorer SFR, it is necessary to show several examples of calibration data.

Figure 6. Dynamics Explorer sweep frequency receiver block diagram.

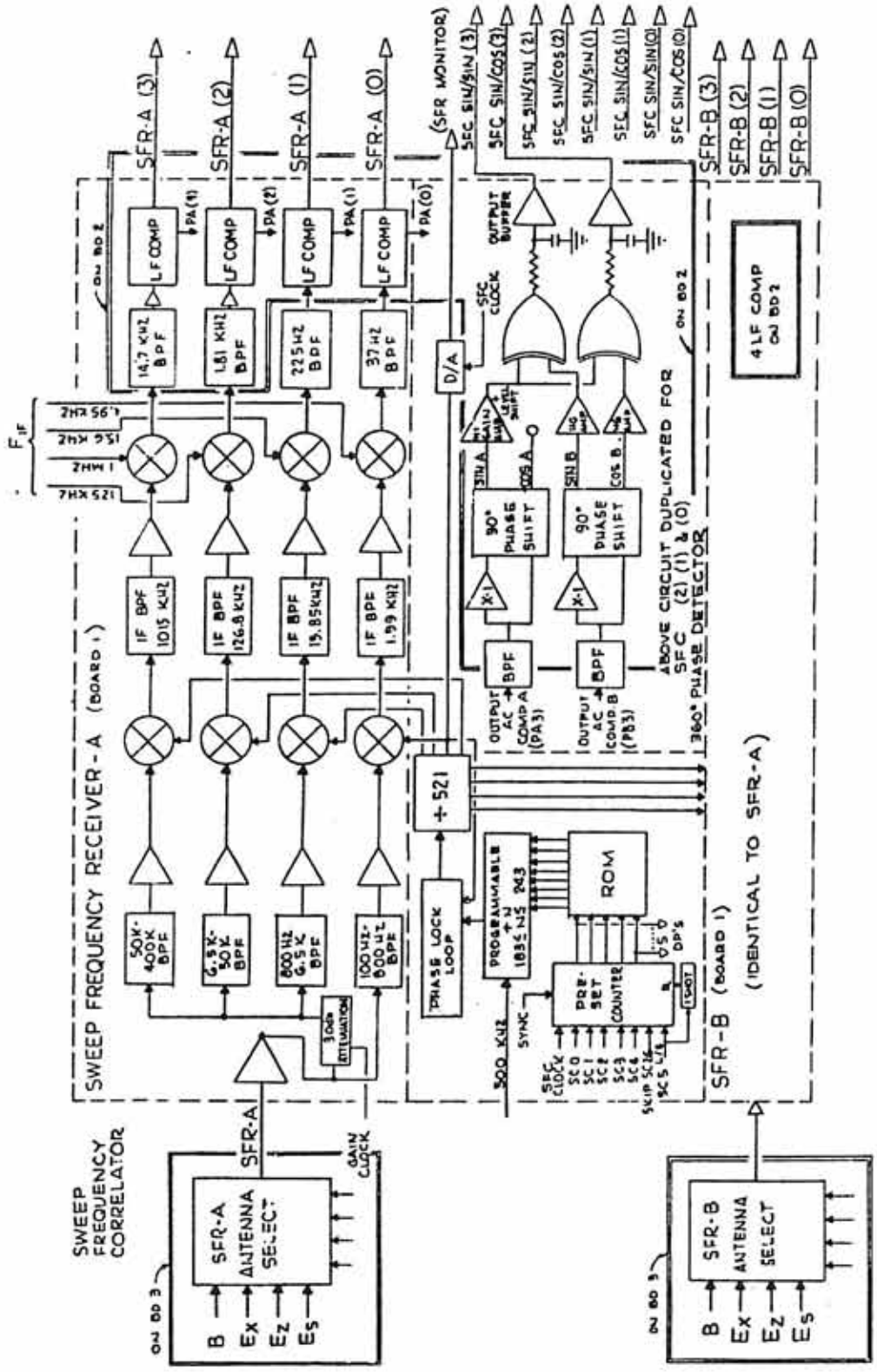
SWEEP FREQUENCY RECEIVER - A (BOARD 1)
SFR-A (3)
SFR-A (2)
SFR-A (1)
SFR-A (0)
LF COMP
14.7 KHZ BPF
1.81 KHZ BPF
225 HZ BPF
37 HZ BPF
IF BPF 1015 KHZ
IF BPF 126.8 KHZ
IF BPF 15.85KHZ
IF BPF 1.99 KHZ
50K-400K BPF
6.5K-50K BPF
800 HZ-6.5K BPF
100 HZ-800 HZ BPF
30db ATTENUATION
PHASE LOCK LOOP
+ 521
PROGRAMMABLE ÷N 1035 NS 243
ROM
PRE-SET COUNTER
500 KHZ
SYNC
SFC CLOCK
SC 0
SC 1
SC 2
SC 3
SC 4
SC 5
SKIP SC 16
D/A
(SFR MONITOR)
SFC SIN/SIN (3)
SFC SIN/COS (3)
SFC SIN/SIN (2)
SFC SIN/COS (2)
SFC SIN/SIN (1)
SFC SIN/COS (1)
SFC SIN/SIN (0)
SFC SIN/COS (0)
OUTPUT BUFFER
90° PHASE SHIFT
X-1
BPF
OUTPUT AC COMP A (PA3)
OUTPUT AC COMP B (PB3)
ABOVE CIRCUIT DUPLICATED FOR SFC (2) (1) & (0)
360° PHASE DETECTOR
4 LF COMP ON BD 2
SFR-B (3)
SFR-B (2)
SFR-B (1)
SFR-B (0)
SFR-B (BOARD 1)
(IDENTICAL TO SFR-A)
SWEEP FREQUENCY CORRELATOR
SFR-A ANTENNA SELECT
SFR-B ANTENNA SELECT
GAIN CLOCK
B
Ex
Ez
Es
ON BD 3

Figure 7 shows a 2-dB amplitude calibration plot of the uppermost channel. The input frequency and both mixing signals are held constant. The amplitude of the incoming signal is decreased in 2-dB increments, from 0-dB referenced to 1V-rms, down to 80 dB below 1 V. The vertical scale is the corresponding DC output. As is evident from the plot, the resulting dynamic range is only about 80 dB.

Figure 8 shows a frequency response plot of the uppermost channel in which the mixing signals and the amplitude of the input signal remain constant while the frequency of the input is varied over a wide frequency range. The 0-dB level plot indicates a large number of spurious responses besides the desired response. Although these spurious responses are unavoidable, it is desirable to reduce them as much as possible. Notice that the -20 dB level is considerably cleaner.

There are two important methods to measure phase accuracy of the SFR. One is to put the same signal into both inputs and vary the frequency of this signal over the passband of a channel, noting the resulting phase offset over this range. Another method is to put broadband noise into the instrument and take note of the resulting phase number at the output following an appropriate sample interval. With this method, the phase error is weighted in accordance with the frequency response of a given channel. More representative of typical signals in many cases then is the simple phase plot vs. frequency.

Figure 7. Dynamics Explorer SFR A3 2-dB calibration. (a) High gain receiver setting. (b) Low gain receiver setting.

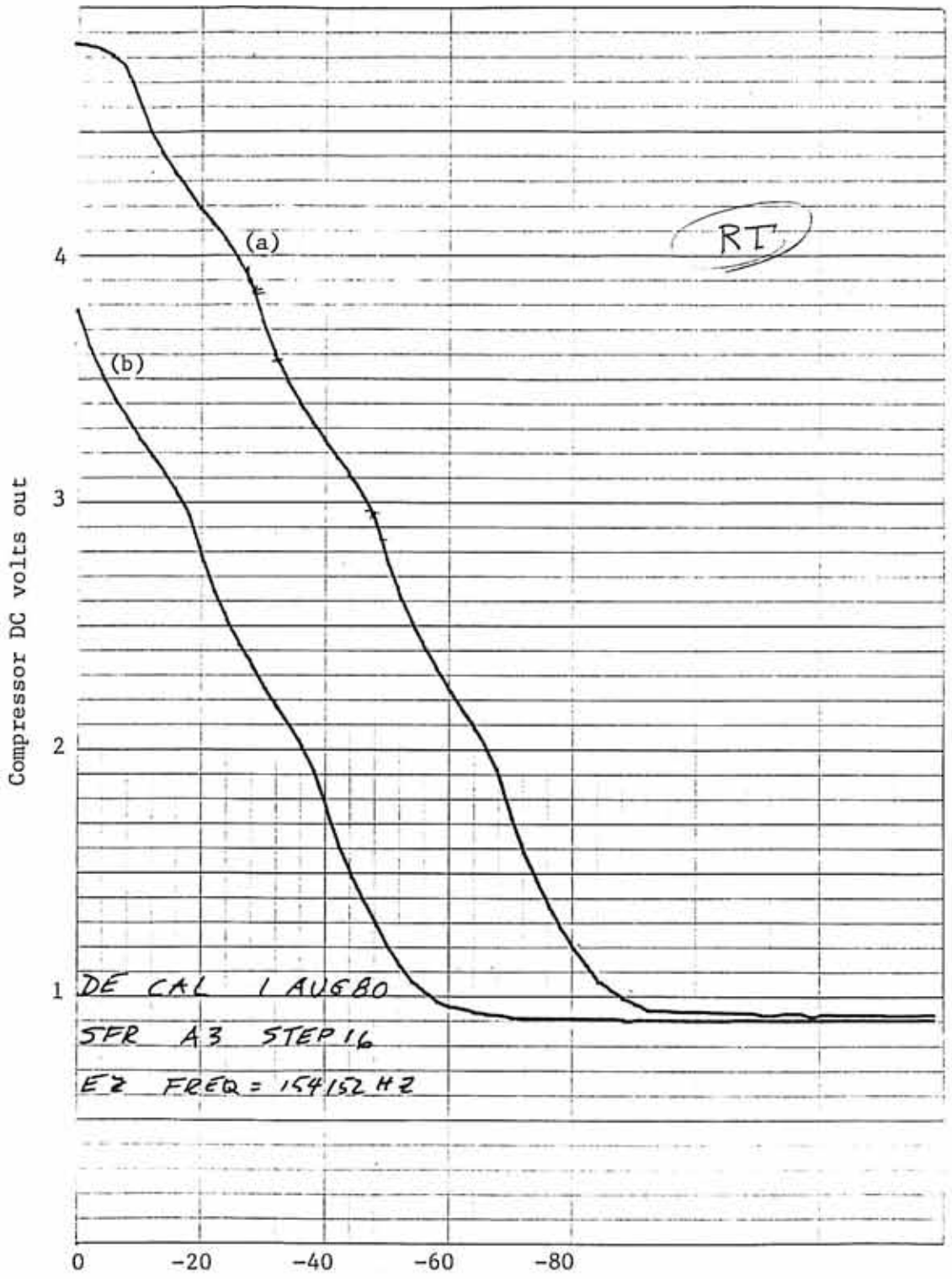
(a)
(b)
RT
DE CAL 1 AUG 80
SFR A3 STEP 16
EZ FREQ = 154152 HZ
Compressor DC volts out
4
3
2
1
0
-20
-40
-60
-80
Attenuation below 1-V rms in decibels

Figure 8. Dynamics Explorer SFR A3 wideband frequency response plot.

Two examples of the former method are illustrated in Figures 9 and 10. The only difference between the two plots is the temperature. Note that the average phase offset range is from approximately 38 degrees for the -15 C plot to nearly 45 degrees for the room temperature (RT) plot.

26.4 MHz Multibaseline Interferometer System

The receiver this section discusses originates from a 1974 thesis from the University of Iowa Physics Department (see Reference 2). It makes use of theory which is widely used in radio astronomy and is presented briefly in this section. This theory relates to the determination of correlation (or fringe visibility amplitude) of a quadrature receiving system and one bit correlator. A quadrature receiver has dual outputs with a relative 90 deg phase shift between them. The outputs are denoted by sine and cosine to indicate the 90 degree phase relation between them.

Figure 11 is the block diagram of the one - bit correlator employed in the 26.4 MHz system. No amplitude information is retained in this one - bit quantization correlation scheme. One bit simply denotes the sign of the signal. The hard limiters turn the continuous waveforms into binary waveforms. The "exclusive - or" circuit cross-correlates the incoming signals with the exclusive - or function. These are then inverted and sent to an integrator to yield a normalized one-bit autocorrelation function.

Figure 9. SFR3 phase difference between bands A and B over the passband. Test performed at room temperature.

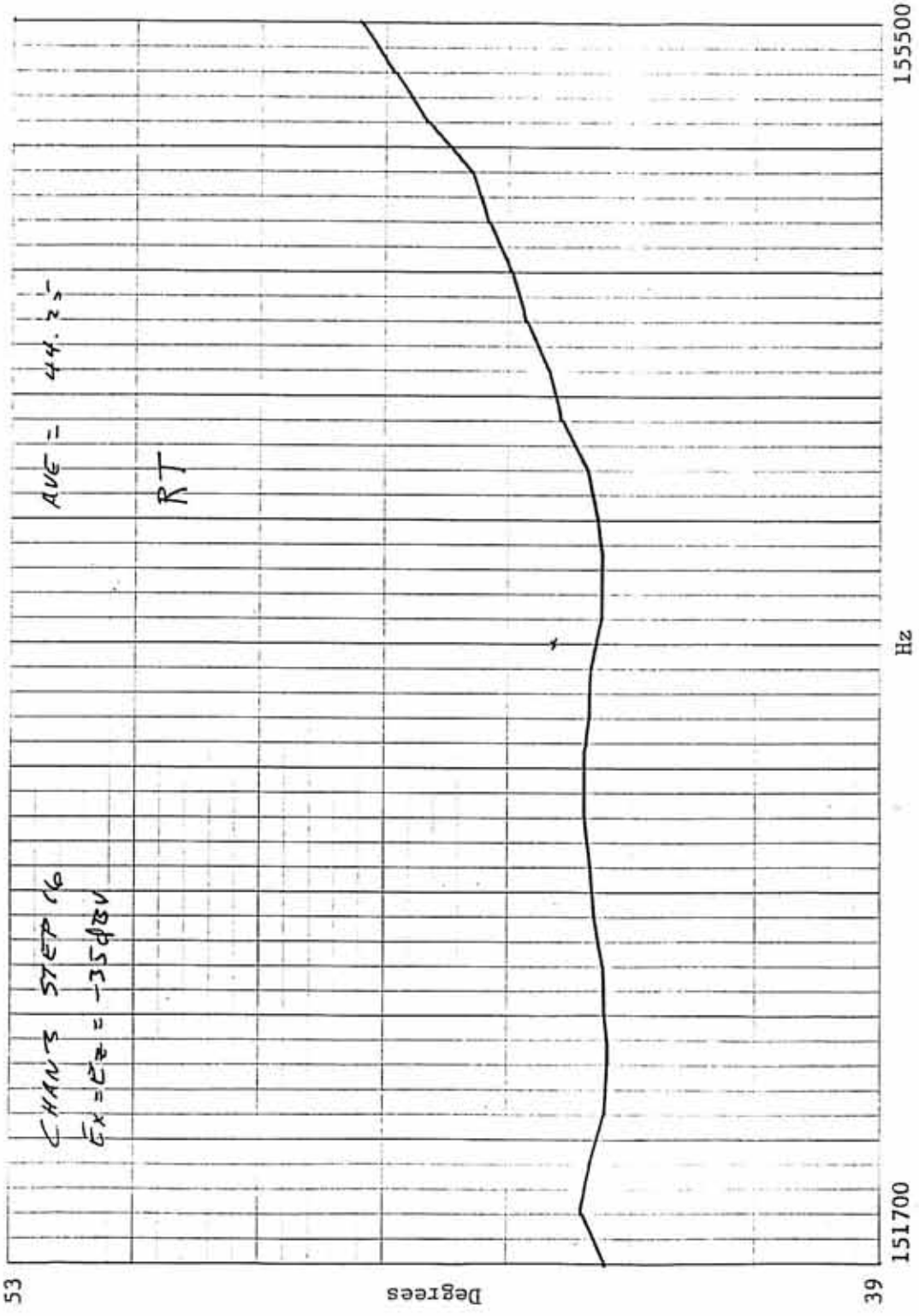
CHAN 3 STEP 16
Ex = Ez = -135dBV
AVE = 44.2
RT
53
Degrees
39
151700
Hz
155500

Figure 10. SFR3 phase difference between bands A and B over the passband. Test performed at -15 C.

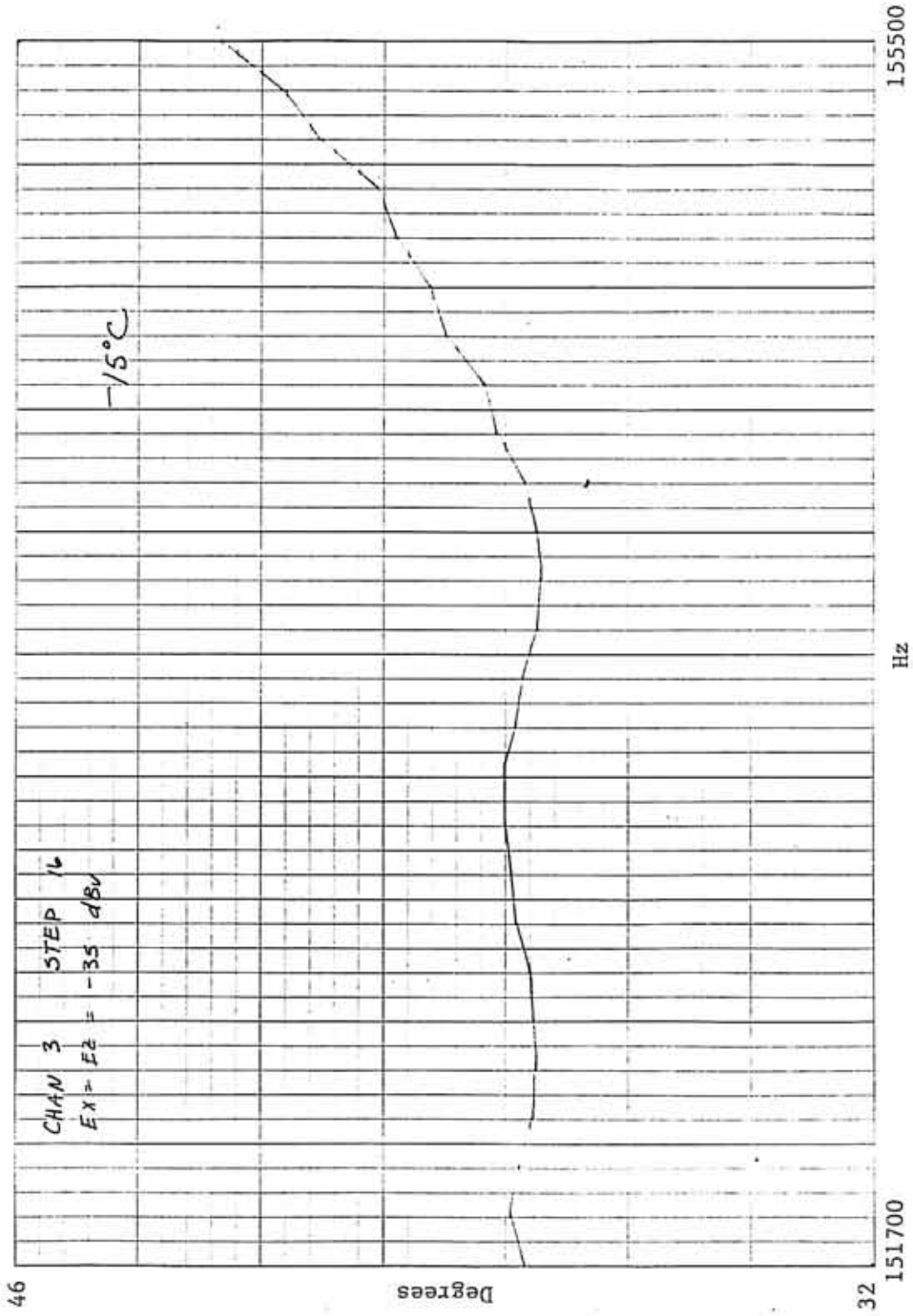
155500
Hz
151700
46
Degrees
32
-15°C
CHAN 3 STEP 16
EX = E2 = -35 dBv

Figure 11. Interferometer receiver block diagrams. (a) 26.4 MHz multibaseline interferometer receiver. (b) 1-bit correlator.

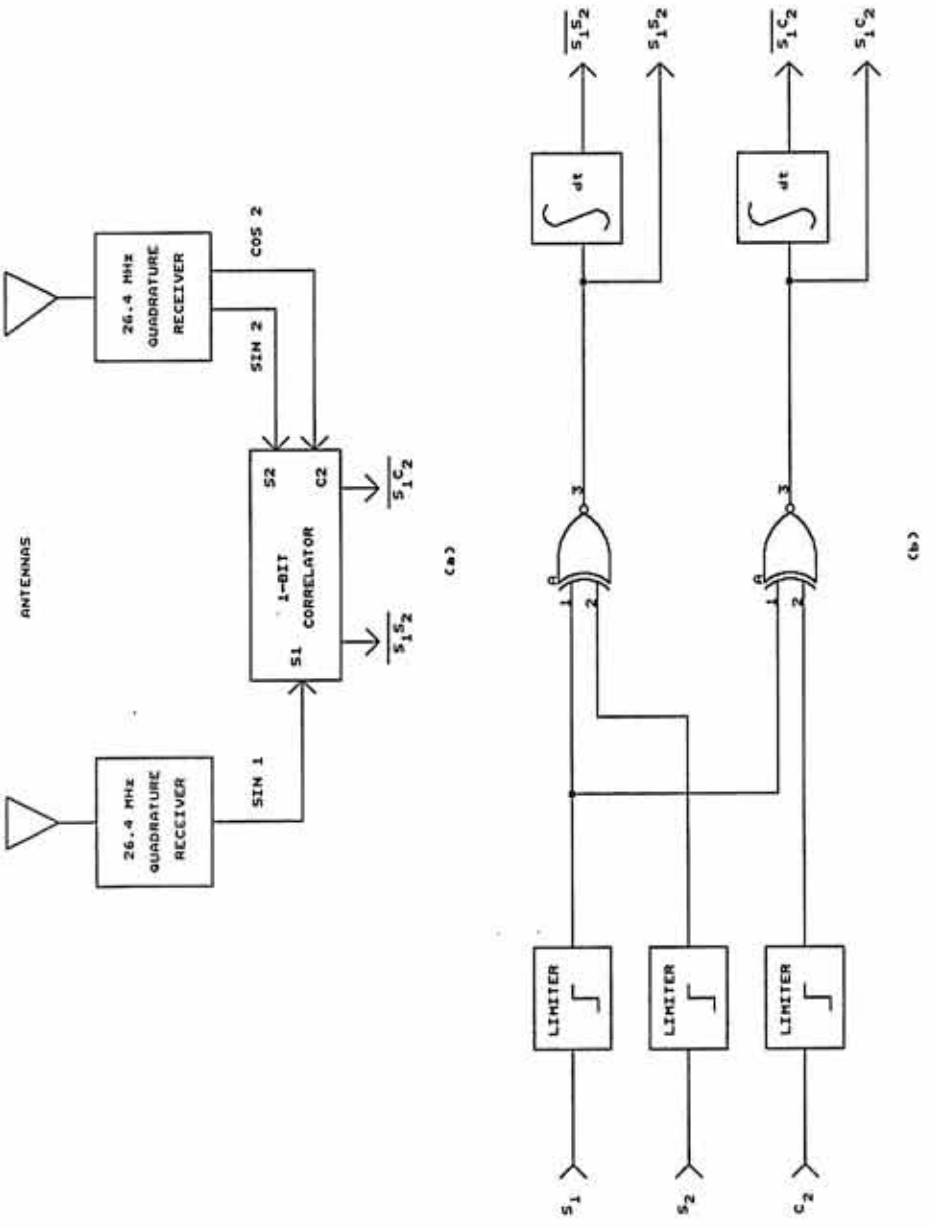
ANTENNAS
26.4 MHz QUADRATURE RECEIVER
26.4 MHz QUADRATURE RECEIVER
SIN 1
COS 2
SIN 2
S1
S2
C2
1-BIT CORRELATOR
$\overline{S_1C_2}$
$\overline{S_1S_2}$
(a)
LIMITER
LIMITER
LIMITER
S_1
S_2
C_2
dt
dt
$\overline{S_1S_2}$
S_1S_2
$\overline{S_1C_2}$
S_1C_2
(b)

DESIGN OF THE INSTRUMENTATION

Overview

As illustrated in Figure 3, there are three band pass filters in the signal path. The purpose of the first, the front-end bandpass filter, is to reduce the bandwidth of the spectrum entering the front of the receiver. Stimulation outside of the desired operating range of a given receiver band may cause spurious responses as harmonics and subharmonics of the offending signal pass through the intermediate frequency filter following the first conversion because of nonlinearities in the first mixer.

The intermediate frequency (IF) filter attenuates frequencies outside of the frequency range that gets mixed to baseband. This results in a substantial reduction of spurious responses which would otherwise reduce receiver performance. The bandwidth of the intermediate frequency filter has an experimentally obtained trade-off between a narrow bandwidth which results in cleaner spurious free response and a wide bandwidth whose phase vs. frequency curve is smoother. A filter with a slowly changing phase curve is preferable from a phase accuracy standpoint because phase matching between filters is easier. The Dynamics Explorer intermediate frequency filter is a narrow filter with a large amount of phase shift over a narrow frequency range, and phase matching is difficult.

The back-end bandpass filter sets the detection bandwidth of the receiver. The filter is approximately an octave wide and the stopband slopes are as sharp as possible without compromising the power dissipation or phase shift characteristics of the filter.

The wideband ninety degree phase shifters provide two outputs differing in phase by ninety degrees. They must provide this phase offset over the bandwidth set by the back-end bandpass filter. It is important that error from ninety degrees be minimized, as phase error will cause a reduction of sideband rejection. Also, the absolute phase shift from the input to the two outputs must be the same for all of the networks otherwise phase mismatch between channels will result.

The front-end mixer steps through a set of logarithmically or linearly spaced frequencies (f1), depending on mode, and over a time interval mixes a set of input frequencies up to a constant intermediate frequency. It is desirable that the first mixer can handle wide bandwidth, high amplitude signals without becoming nonlinear. Nonlinearity will result in intermodulation distortion and spurious responses.

The second mixer, using f2 to convert the IF signal to baseband, is less critical in this respect although it is important that the harmonic distortion of the second mixer amplifier A2 be as low as possible. Harmonics produced in A2 do not contain the proper phase

quadrature relationship for sideband reduction using the phase shifting method.

Finally, the logarithmic compressor consists of a chain of five amplifiers in cascade and the output of each enters into the summing node of a full wave detector amplifier. The output of the detector is a DC voltage between 0 and 5 volts proportional to the logarithm of the input signal level. The design of the amplifiers themselves will not be discussed in detail as they are identical to those in the Dynamics Explorer instrument. A considerable amount of time will be spent discussing the time constant determining components in the compressors. These determine the speed with which the receiver can respond to changing mixing frequencies and input stimuli.

Design of Front-End Filters

Figure 12 shows the SFR1 front-end filter which is topologically identical to that in SFR2 and SFR3. The scaling of break frequency determining components differ from channel to channel. The high frequency cutoff slope is a fifth order Butterworth and is provided by the first two stages. Capacitor C16 and the loading of the next stage provide a first order highpass cutoff. The lowpass cutoff is sharper because there is often more energy at higher frequencies to be attenuated. The current through the transistors is set by constant current field effect transistors D3 and D4. These FET's are two terminal devices with the gate internally connected to the source

Figure 12. Schematic of SFR-1 front-end filter. The same topology is used for SFR-2 and SFR-3.

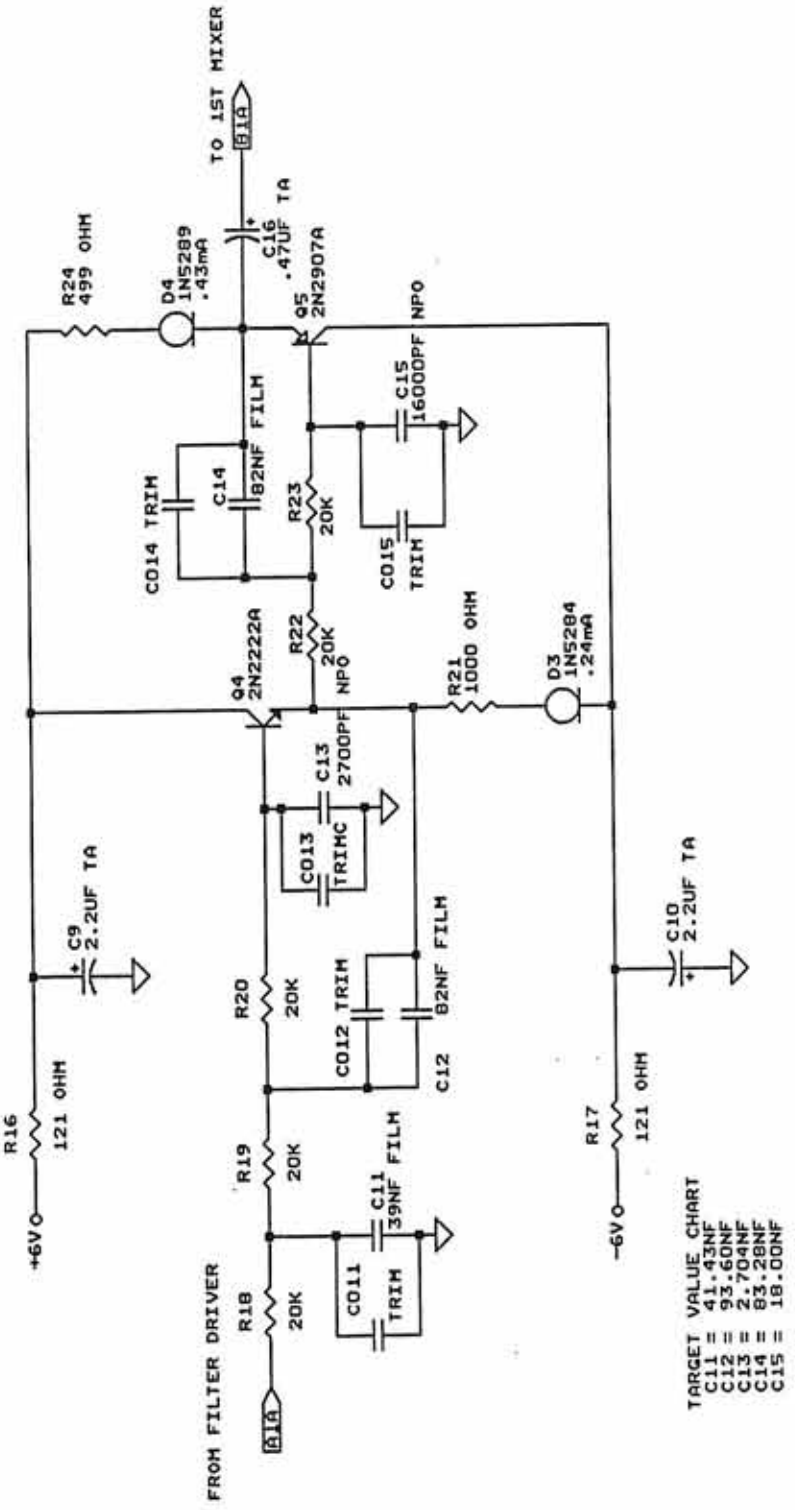
TO 1ST MIXER
R24 499 OHM
D4 1N5289 .43mA
C16 .47UF TA
Q5 2N2907A
C15 1600PF NPO
C14 82NF FILM
C014 TRIM
R23 20K
C015 TRIM
Q4 2N2222A
R22 20K NPO
R21 1000 OHM
D3 1N5284 .24mA
C13 2700PF
C013 TRIMC
C9 2.2UF TA
R20 20K
C012 TRIM
C12 82NF FILM
C10 2.2UF TA
R16 121 OHM
+6V
R19 20K
C11 39NF FILM
C011 TRIM
R17 121 OHM
-6V
R18 20K
FROM FILTER DRIVER
TARGET VALUE CHART
C11 = 41.43NF
C12 = 93.60NF
C13 = 2.704NF
C14 = 83.28NF
C15 = 18.00NF

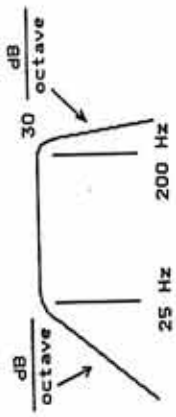
dB
30 octave
200 Hz
25 Hz
dB
6 octave

such that the resulting current is Idss. The power consumption of this stage is

$$(.24\ \text{mA} + .43\ \text{mA})(6\ \text{V} + 6\ \text{V}) = 9.04\ \text{mW} \qquad (7)$$

The noise appearing at the output is approximated by the thermal noise of resistors R18 - 23. In the filter passband these resistors appear in series and the equivalent noise bandwidth of this channel, as set by the back-end filter, is 10 Hz. The thermal noise is:

$$\left(\frac{4\ \text{nV}}{\sqrt{\text{Hz}\cdot\text{k}\Omega}}\right)(\sqrt{20\ \text{Hz}})(\sqrt{100\ \text{k}\Omega}) = .179\ \text{uV} \qquad (8)$$

Figure 13 illustrates the SFR4 front-end filter which is similar in topology to that in SFR5. It is a third order Butterworth highpass section followed by an elliptical lowpass. Again, a large rejection of frequencies above the passband reduces the high amplitude, high frequency signals often received by the electric antennas.

Temperature stability of components is especially critical in this filter. The sharp elliptical filter causes a large amount of phase shift. The series inductors, their parasitic capacitance, and C13 and C14 determine the frequency of the zeros that cause deep nulls immediately above the corner frequency. A large group delay is associated with these zeros. It has been found experimentally that

Figure 13. SFR-4 front-end filter. A filter of similar topology is used in SFR-5.

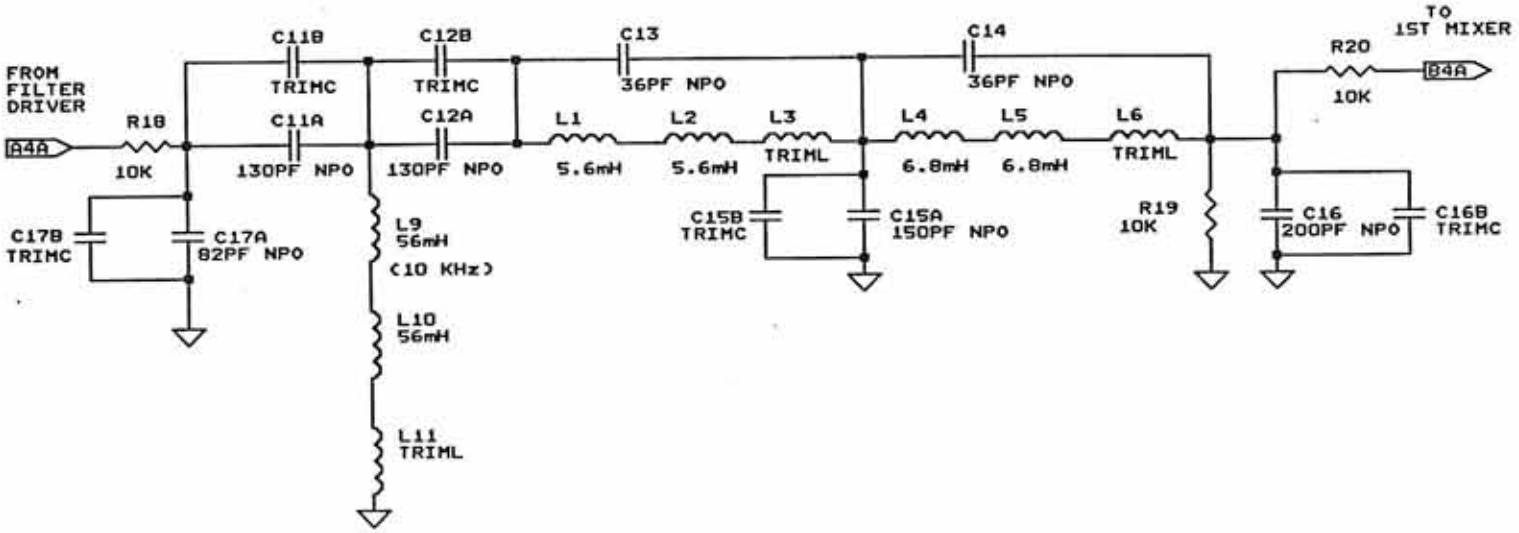

3. C11,C12 TARGET VALUE 1376PF
   C15 TARGET VALUE 156.8PF
   C16 TARGET VALUE 206.6PF
   C17 TARGET VALUE 84.4PF.

2. L1, L2, L3 TARGET VALUE 13.40mH
   L4, L5, L6 TARGET VALUE 14.55mH.
   L9, L10, L11 TARGET VALUE 122.5mH

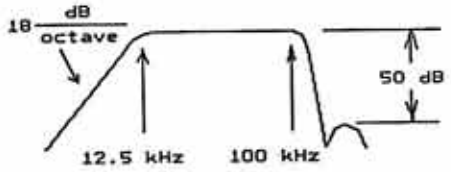

after a large number of temperature cycles, the value of inductance becomes stable in that when the value at a given temperature is noted and the temperature is cycled and then returned to its starting value, the inductance is its initial value. The NPO dielectric capacitors have a temperature coefficient of 30 ppm/deg C and this is generally better then the inductors.

Design of Intermediate Frequency Filters

Figure 14 shows the IF filter for SFR1. It is identical in topology to those in SFR2 and SFR3. It is especially important that the attenuation above the passband be sufficiently high so that the third harmonic of the first mixing signal be reduced by at least 40 dB in comparison to the fundamental. The attenuation above the passband in this filter is 30 dB per octave and, assuming no peaking, the attenuation of the third harmonic of 490 Hz (1470 Hz) is 47.5 dB. Since each of the two last sections of the filter are considerably under damped, the actual attenuation rate is somewhat higher then 30 dB per octave in the first octave above 490 Hz.

The use of two transistors per stage instead of single transistor buffers is necessary because current gain must be high enough so the highly peaked stages work according to theory. Exactly how high it must be is difficult to predict but by trial and error the transistor betas in the compound configuration had to drop below about 10 before the shape of the peak began to change appreciably. Minimum current gains of around 10 for individual transistors is not

Figure 14. SFR-1 intermediate frequency filter.

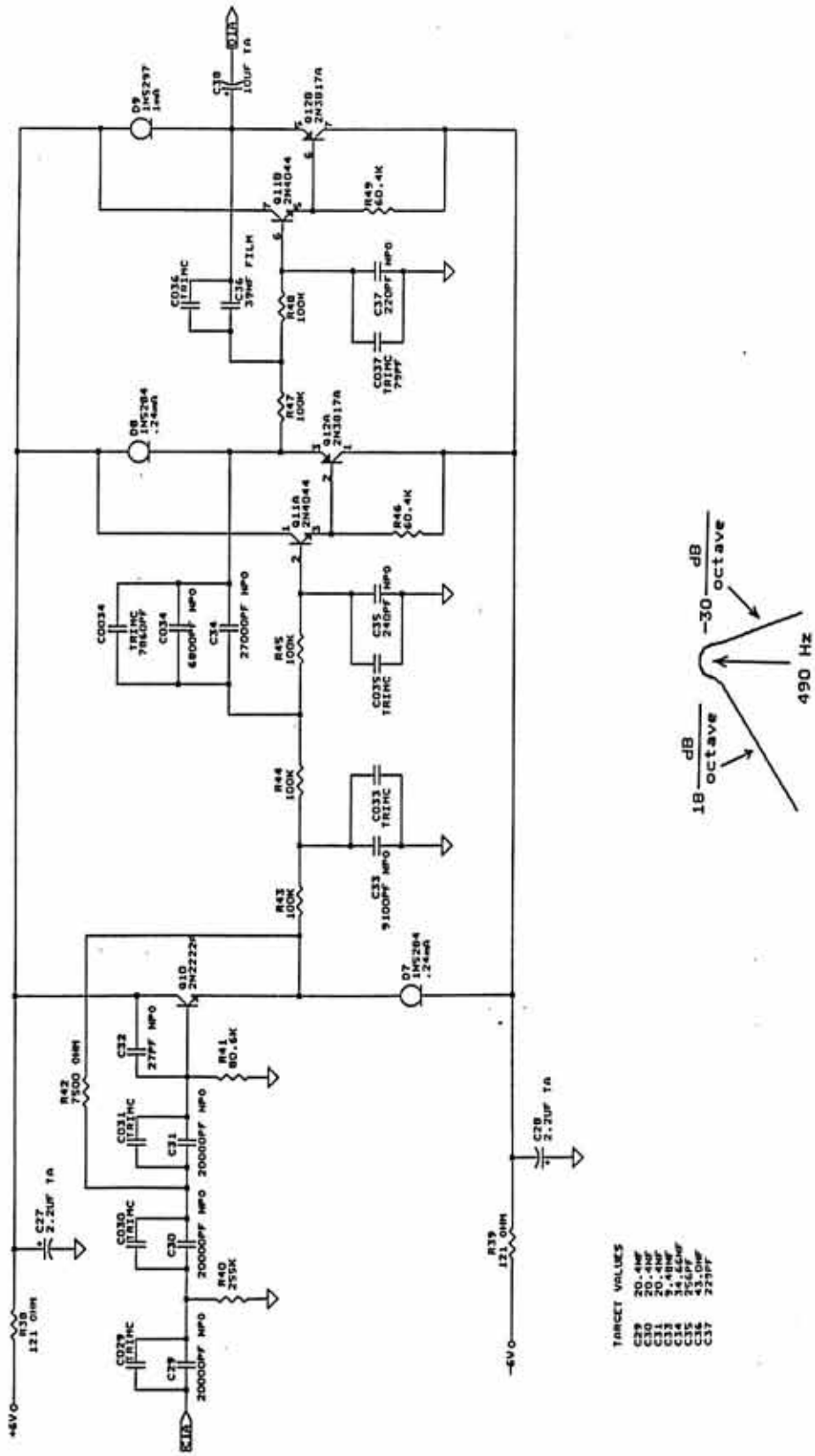
+6V
-6V
OUT
IN
C27 2.2UF 1A
C28 2.2UF 1A
C29 20.4NF
C30 20.4NF
C31 20.4NF
C33 9.48NF
C34 3.66NF
C35 1.06NF
C36 43.0NF
C37 229PF
18 dB octave
-30 dB octave
490 Hz

unrealistic under worst case conditions of extended radiation exposure and cold temperatures. The power consumption of this stage is calculated as before for the front-end filter and is 20.2 mW.

The SFR4 IF filter, shown in Figure 15, is similar in topology to that in SFR5. Although the asymptotic upper attenuation rate is only 12 dB per octave, the filter has a large amount of peaking around the center frequency. The transfer function for this filter is:

$$\frac{V_o}{V_I} = \frac{S/C_{30}R_{42}}{S^2 + \frac{S}{C_{30}}\left(\frac{R_{42} + R_{43}}{R_{42}R_{43}}\right) + \frac{1}{L_8C_{30}}} \qquad (9)$$

The damping is controlled by both resistors and the center frequency is set by the LC combination.

Design of Back-End Bandpass Filters

Table 1 shows the SFR step times, detection center frequencies, and detection bandwidths. The SFR5 back-end center frequency is 10 kHz and the bandwidth is 8 kHz. Both of these are established by the back-end filter. The SFR5 frequency parameters are divided by eight for SFR4. Similarly, SFR3 represents a division from 4 and SFR2 is a division from 3. Continuing in this way, SFR1 would have a back-end center frequency of 2.4 Hz and a bandwidth of 2 Hz. This back-end frequency was found to be too low to be realizable with reasonable component values. Additionally, a bandwidth of only 2 Hz requires more then 1.04 seconds for complete settling of the output. Both the

Figure 15. SFR-4 intermediate frequency filter.

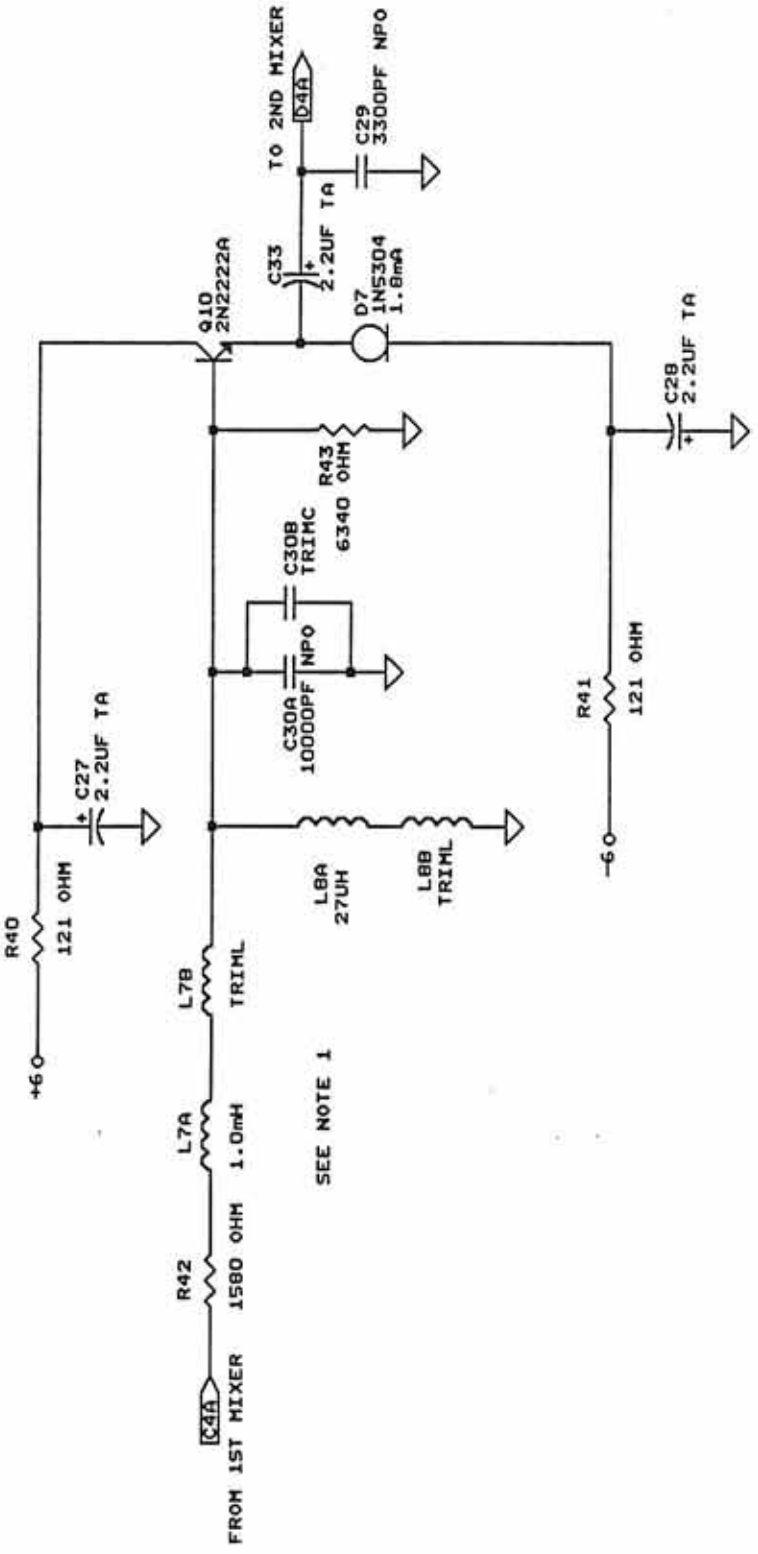

1. INDUCTORS ARE MIL-C-M39010/03
   L7 1.013mH INDUCTOR MADE UP OF 1.0mH + TRIM
   L8 40.5UH COIL MADE UP OF 27UH + TRIM.

2. TARGET VALUE C30 = 10.2NF (10200PF)

Table 1. SFR Step Times and Center Frequencies

SFR	1	2	3	4	5
Step time	1.04s	52s	280ms	40ms	40ms
Backend frequency	10 Hz	19.5Hz	156Hz	1.25KHz	10KHz
Detection Bandwidth	5Hz	15.6 Hz	125Hz	1.0KHz	8.0KHz
Figure of merit	.0096	.0375	.5571	31.25	250

center frequencies and the detection bandwidths were compromised here to make this channel realizable.

Two back-end filter topologies are employed in this receiver. Figure 16 illustrates the topology used in SFR2 through SFR5. It is symmetrical with fifth order high and low pass slopes and has a bandwidth of just over two octaves. With the exception of capacitors 101 through 110 which are scaled for the different frequencies, each filter is identical. The power dissipation, again calculated by multiplying the current as set by the current diodes by the power supply voltage, is 23 mW.

The back-end filter for SFR1 has a smaller detection bandwidth then that for the other channels. Additionally, the roll-off above the passband is as sharp as is practical because the center frequency is at a relatively high frequency and because of this, the total system is not as selective. Figure 17 illustrates the back-end filter employed for SFR1. It is similar in design to the other channels except that it has six instead of four stages. The result

Figure 16. SFR-2 back-end bandpass filter. SFR-3 through SFR-5 employ the same topology.

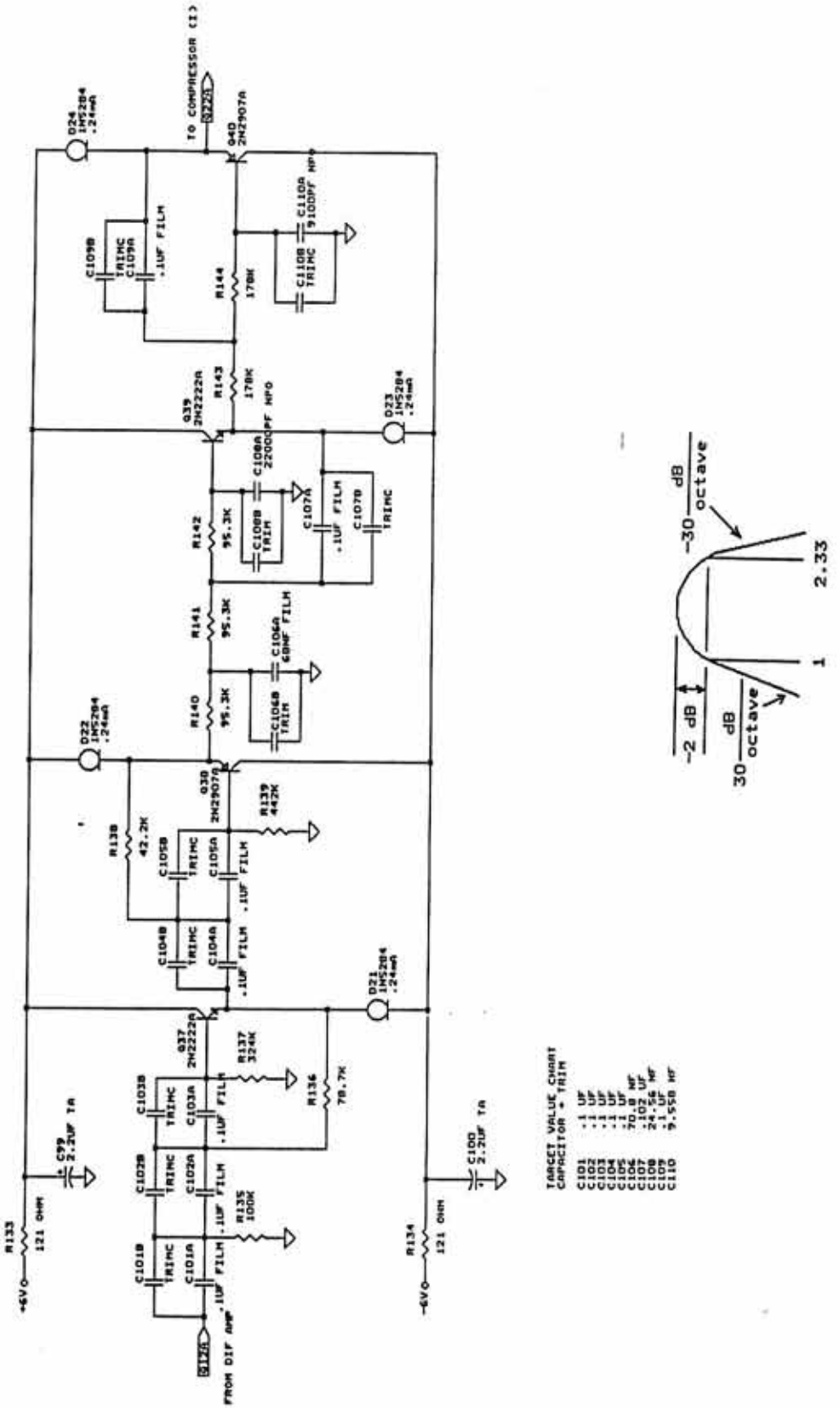
TO COMPRESSOR (I)
FROM DIF AMP
+6V
-6V
121 OHM
2.2UF TA
.1UF FILM
TRIMC
TRIM
68NF FILM
2200PF MPO
9100PF MPO
42.2K
95.3K
178K
442K
324K
100K
78.7K
-30 dB/octave
-2 dB
30 dB/octave
1
2.33
TARGET VALUE CHART
CAPACITOR + TRIM
C101 .1 UF
C102 .1 UF
C103 .1 UF
C104 .1 UF
C105 .1 UF
C106 .068 MF
C107 .1 UF
C108 24.56 MF
C109 .1 UF
C110 9.558 MF

Figure 17. SFR-1 back-end filter.

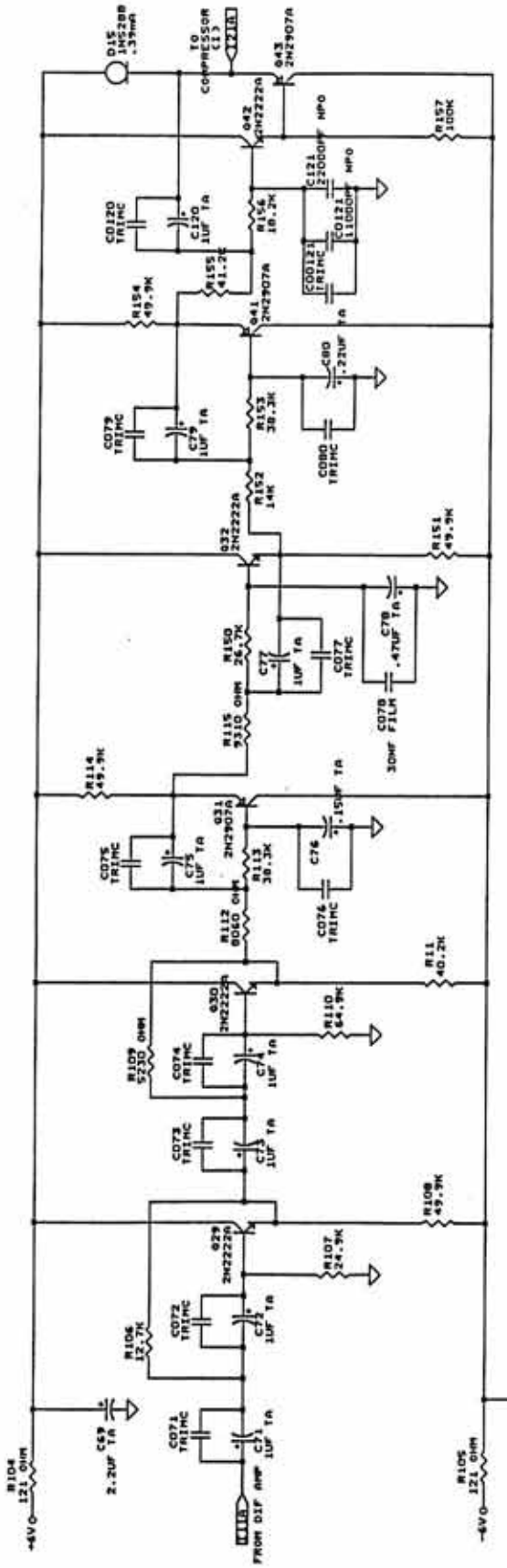
D15 1N5288 .39mA
TO COMPRESSOR (13)
Q43 2N2907A
Q42 2N2222A
R157 100K
C121 2200pF NPO
C0121 TRIMC
C120 1UF TA
C0120 TRIMC
R156 18.2K
R155 41.2K
R154 49.9K
Q41 2N2907A
C80 .22UF TA
C0 TRIMC
C79 1UF TA
C079 TRIMC
R153 39.2K
R152 14K
Q32 2N2222A
R151 49.9K
C78 .47UF TA
C078 30MF FILM
C77 1UF TA
C077 TRIMC
R150 26.7K
R115 5310 OHM
R114 49.9K
Q31 2N2907A
C75 1UF TA
C075 TRIMC
C76 .15UF TA
C076 TRIMC
R113 30.1K
R112 8060 OHM
R11 40.2K
Q30 2N2222A
R110 64.9K
C74 1UF TA
C074 TRIMC
R109 5230 OHM
C73 1UF TA
C073 TRIMC
R108 49.9K
Q29 2N2222A
R107 24.9K
C72 1UF TA
C072 TRIMC
R106 12.7K
C71 1UF TA
C071 TRIMC
R104 121 OHM
+4V
C69 2.2UF TA
FROM DIF AMP (11)
R105 121 OHM
-4V
C70 2.2UF TA
TARGET VALUE CHART
PARALLEL TRIM CAPACITOR REQUIRED TO MATCH EXACT VALUE
C71 = 1UF
C72 = 1UF
C73 = 1UF
C74 = 1UF
C75 = .15UF
C76 = 1UF
C77 = .1UF
C78 = .47UF
C80 = .22UF
C120 = 1UF
C121 = 33MF

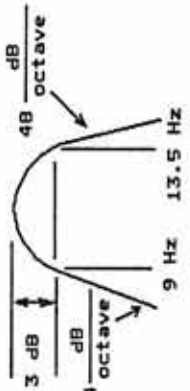
dB
48 octave
13.5 Hz
9 Hz
3 dB
dB
24 octave

is a high upper roll-off rate of 48 dB per octave, as compared to 30 dB per octave for the other channels.

Design of Ninety-Degree Phase Shifters

Figure 3 shows the location of the 90°-phase shifters in the receiver. For the best sideband reduction, it is necessary to have a wideband phase shift which extends beyond (above and below) the back-end detection band. The method of phase shifting chosen here is based on an optimized RC passive network. According to theory outlined by Weaver (see Reference 3), there is an optimal location for the real poles in the left hand plane and the zeros in the right hand plane such that for a given number of singularities, the phase response is as flat as possible over a wide frequency range. It is impossible to design a phase shifter with exactly ninety degrees over a continuous range of frequencies. A phase shifting network will always have a frequency dependent error. This error determines the maximum amount of undesired sideband reduction. For a lower sideband reduction of 40 dB, the maximum phase error is 1 degree.

Design of Mixers

The front-end mixer input generally has several simultaneous high amplitude frequencies present at once. This is especially true in the case of SFR4 and SFR5 where the input bandwidth set by the front-end filter is wide and strong AKR emissions are often detected by the electric antennas. A double balanced mixer scheme is employed

where the mixer switch switches between a pair of resistors connected to alternate ends of a transformer. The amplitude at the switch is kept small because the switch operates into a virtual ground node of an amplifier. Figure 18(a) shows the front-end mixer block diagram.

Switching speed becomes an important consideration in SFR4 and SFR5. A CMOS CD4066 switch, used in the other channels, will not switch fast enough here. The solution is to use a gallium arsenide FET switch arrangement (Figure 19). This device is used to switch a current into a virtual ground as shown in the first part of Figure 18. The output of the SFR-5 mixer, even when switching at 2.8 MHz, displays very fast rise times which are a very short portion of a switching period. This is important since distortion in the first mixer causes spurious responses at subharmonics of the desired detection frequency. For example, a large amount of second harmonic distortion in the first mixer will cause a spurious response at 400 kHz if 800 kHz is the desired detection frequency.

The back-end mixers down convert the IF signal using f2. Their output is a large voltage at the back-end frequency. The back-end mixer's output must be high in amplitude because of the attenuation present in the ninety-degree phase shifters which follow. It would be possible to use more amplification after the phase shifters but since the impedance levels are generally high in these circuits, there would be a large amount of amplification of resistor thermal noise and other noise radiated into the phase shifters.

Figure 18. General mixer topologies. (a) Second mixer for channels 4 and 5, and all first mixers. (b) Second mixer for channels 1 through 3.

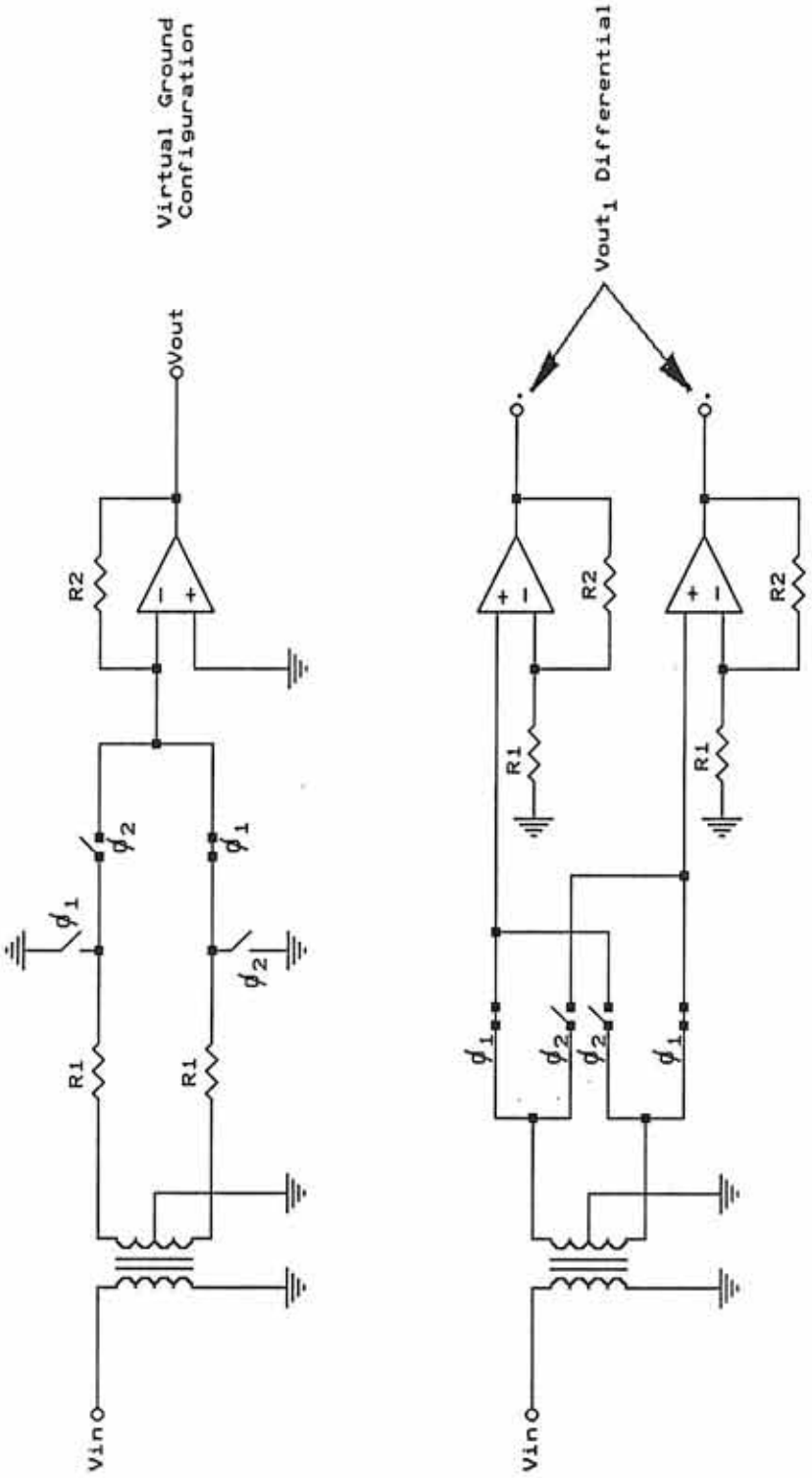
Virtual Ground Configuration
Vout
R2
R1
R1
ϕ_1
ϕ_2
ϕ_2
ϕ_1
ϕ_1
Vin
$Vout_1$ Differential
R2
R2
R1
R1
ϕ_1
ϕ_2
ϕ_2
ϕ_1
Vin

Figure 19. Gallium arsenide mixer configuration.

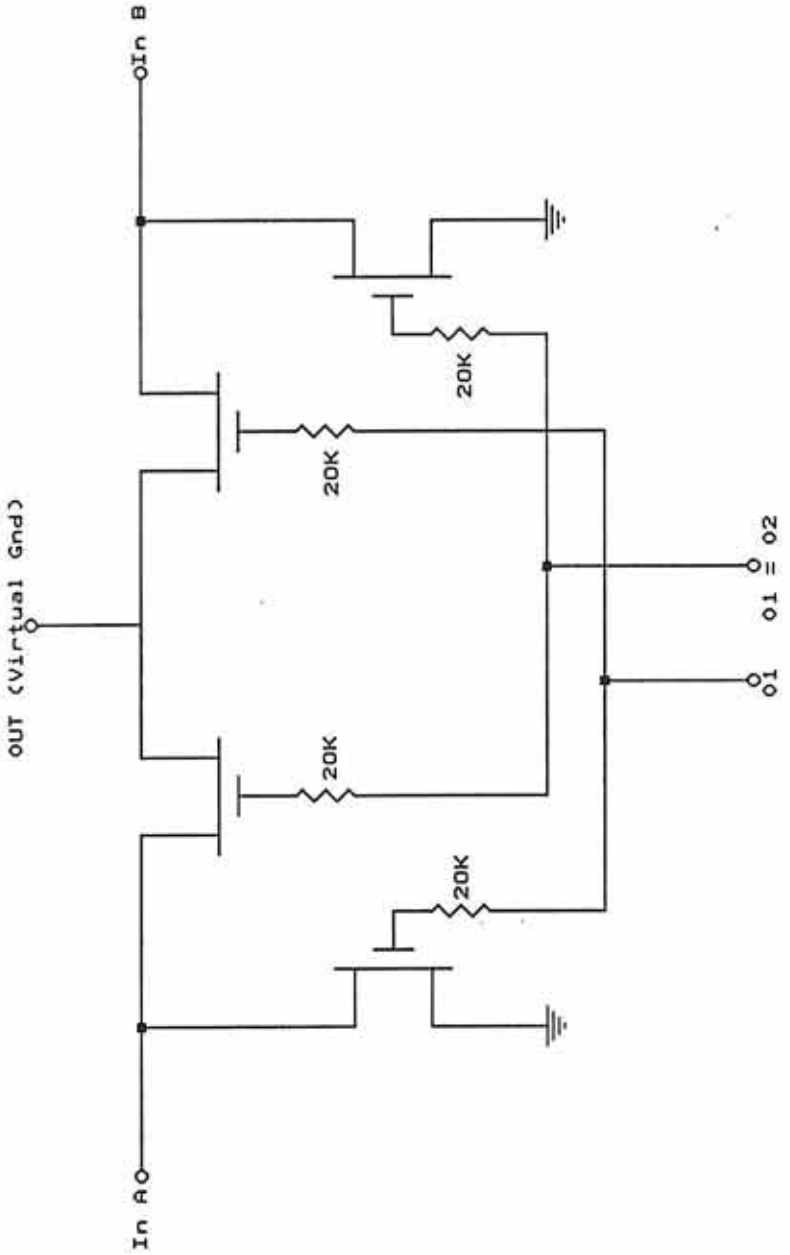
In B
20K
20K
OUT (Virtual Gnd)
Φ1 = Φ2
Φ1
20K
20K
In A

Another consideration of the back-end mixer is harmonic distortion minimization. Harmonics present in this output do not have the correct quadrature relationship, unlike the fundamental, and are not canceled as they should be (Appendix 2). Figure 18(a.b) shows the topologies used for the second mixer, again with each one optimized for a specific frequency range.

Design of Compressors

A discussion of the compressors is necessary to understand their effect on receiver response time and phase response. They are considerably slower than the group delay of the back-end filters which set the detection bandwidth and therefore determine the speed at which the receiver operates.

Figure 20(a) illustrates a block diagram of the compressor. It is constructed of hybrid amplifiers and a summing amp/detector as well as a number of coupling and time constant capacitors whose values are determined by the desired frequency of operation and response time. The input signal runs into this series of amplifiers, and depending on its amplitude, one or more are driven into clipping. When the outputs of each amplifier are summed together, the result is a waveform whose peak value is approximately proportional to the logarithm of the input. This waveform is sent into the full-wave peak detector shown in Figure 21. The final result is a d.c. voltage proportional to the log of the input amplitude.

Figure 20. Logrithmic compressor. (a) Block diagram.
(b) X 5.5 amplifier schematic.

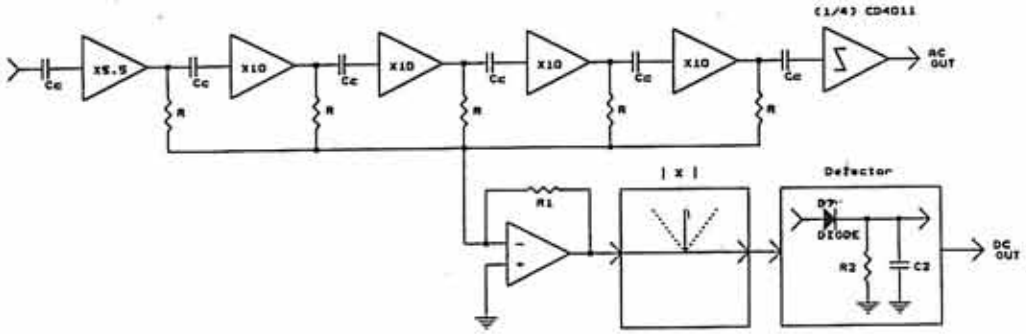
(1/4) CD4011
X5.5
X10
X10
X10
X10
Cc
R
AC OUT
| X |
Defector
R1
D1
DIODE
R2
C2
DC OUT

(a)

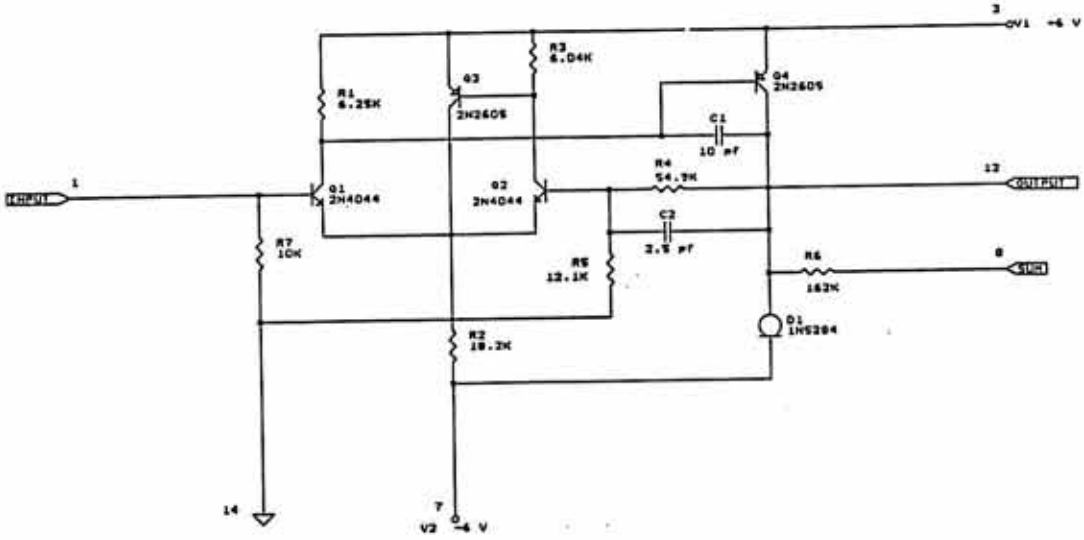
3
CV1 +6 V
R3 6.04K
Q3 2N2605
Q4 2N2605
R1 6.25K
C1 10 pf
1
Q1 2N4044
Q2 2N4044
R4 54.9K
12
C2 2.5 pf
R7 10K
R5 12.1K
R6 162K
8
D1 1N5284
R2 18.2K
14
7
V2 -6 V

(b)

Figure 21. Full wave detector for compressor.

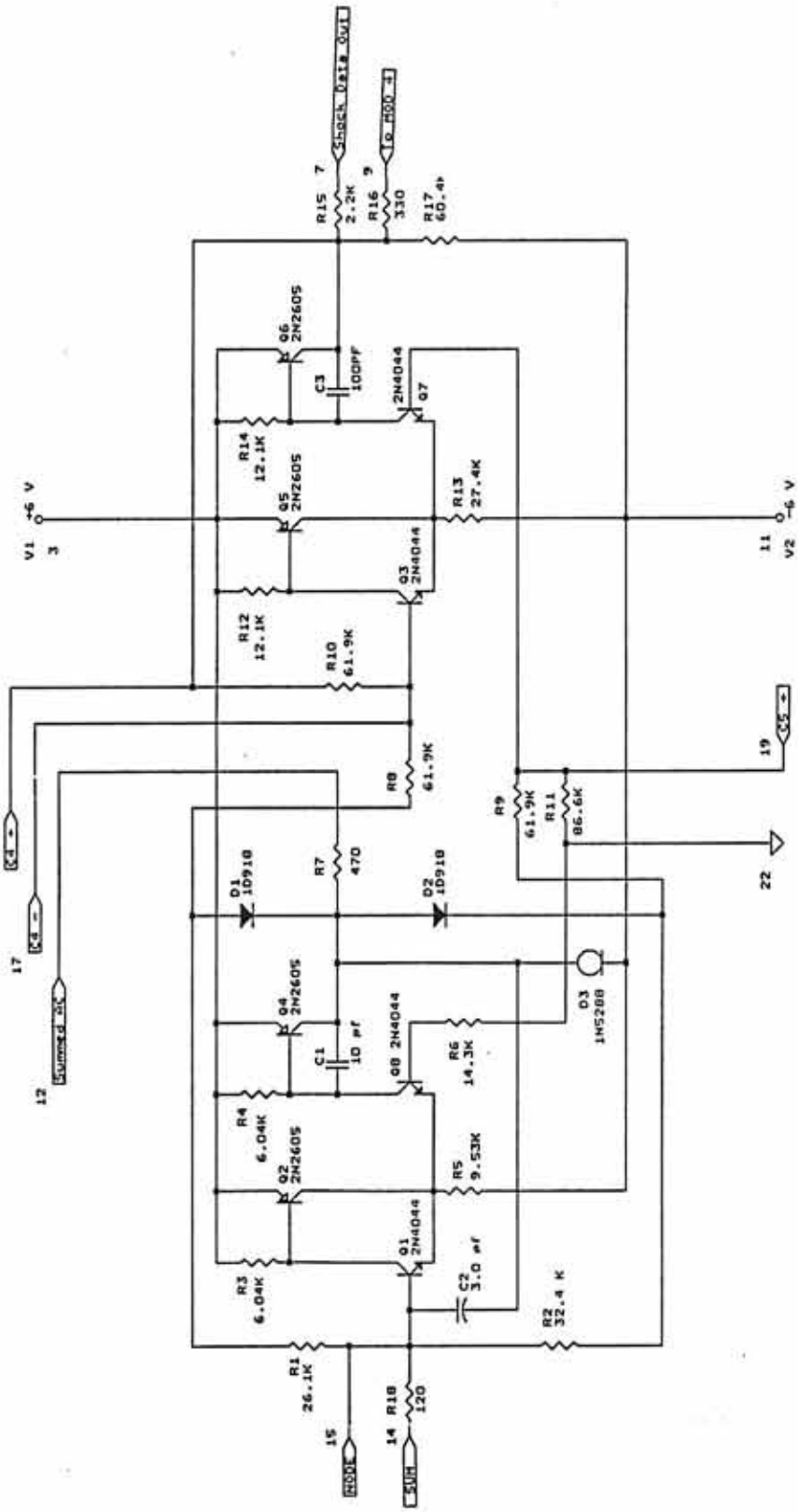
Shock Data Out
Q_RSD -I
R15 7
2.2K
R16 9
330
R17
60.4K
Q6 2N2605
C3
100PF
2N4044 Q7
R14
12.1K
Q5 2N2605
R13
27.4K
+6 V
V1
3
+6 V
11
V2
Q3 2N4044
R12
12.1K
R10
61.9K
R8
61.9K
19
CS -
R9
61.9K
R11
86.6K
22
6
CS -
17
CS -
12
Summed Alt
D1 1D918
R7
470
D2 1D918
D3 1N5288
Q4 2N2605
C1
10 pf
Q8 2N4044
R6
14.3K
R4
6.04K
Q2 2N2605
R5
9.53K
Q1 2N4044
C2
3.0 pf
R3
6.04K
R2
32.4 K
R1
26.1K
15
RSD -I
14 R18
120
SUM

Each amplifier in Figure 20(a) is separated by a coupling capacitor which introduces an undesirable phase shift. AC coupling is necessary to prevent the small offset voltages present on the amplifier outputs at the front of the chain from getting amplified by a large factor and saturating the amplifiers at the back of the chain.

The size of these capacitors sets a limit on how fast the chain can respond to a change of input signal level intensity. The reason can be understood in terms of the level dependent DC offsets, especially those of the amplifiers at the front of the chain. When the amplifier is operating in the linear mode, a DC offset voltage appears at the output which is equal to the difference in the Vbe's of the input differential pair multiplied by the closed loop gain. When the amplifier is driven into hard clipping, the average DC level appearing at the output is due to the fact that the clipping is not perfectly symmetric. When the input intensity goes abruptly from a level which has most or all of the amplifiers clipping to a much lower level, the change in DC offsets at the input cascades to the output and holds the final amplifiers in saturation until the coupling capacitors towards the beginning of the chain charge to new values. The end result is a delay in the time for a stabilized signal to appear at the AC output and all of the summing nodes.

For the DC output, a further delay results from the selection of the RC time constant in the detector. The compromise is between a

sufficiently long time constant such that there is negligible droop between cycles and a short enough time constant to allow the full response by the conclusion of a step interval. Twenty mV is the practical resolution limit because of the 8-bit A/D conversion of the 0 to 5V DC voltage. It is therefore desirable that the droop be less then 20 mV and that the DC output voltage be within 20 mV of the final steady-state value.

A measure of the compromises faced by the coupling capacitors and the detector capacitors may be obtained by dividing the back-end frequency in Hz by the step time in ms. These figure of merits are given in Table 1. SFR-1 gives .0096 and SFR-3 gives .5571. SFR-1 represents a very difficult compromise because of the small number and SFR-3 represents a more intermediate compromise.

Figure 22 shows the compressor amplifier chain output following the removal of the input signal at t=0. Waveform (a) is the removal of a 1 v rms saturation level input voltage. Waveform (b) is the removal of a .1 v rms input. The saturation level plot shows a 2.5 second delay to pull out of saturation. The .1 v plot shows a 1.2 second delay. The .01 v level, shown in Figure 23, shows only a .3 second delay after which a phase correlation may begin. Figure 24 and Table 2 show the phase shift through the compressor chain as a function of input level.

Figures 25 and 26, and Table 3 show the same plots and tables for SFR-3. Note that the response times are considerably less then

Figure 22. SFR-1 compressor amplifier chain output following removal of input at t=0. (a) 3.3 uF coupling capacitors, 10 Hz, 0 dB ref. 1 V rms input. (b) 3.3 uF coupling capacitors, 10 Hz, -20 db ref. 1 V rms input.

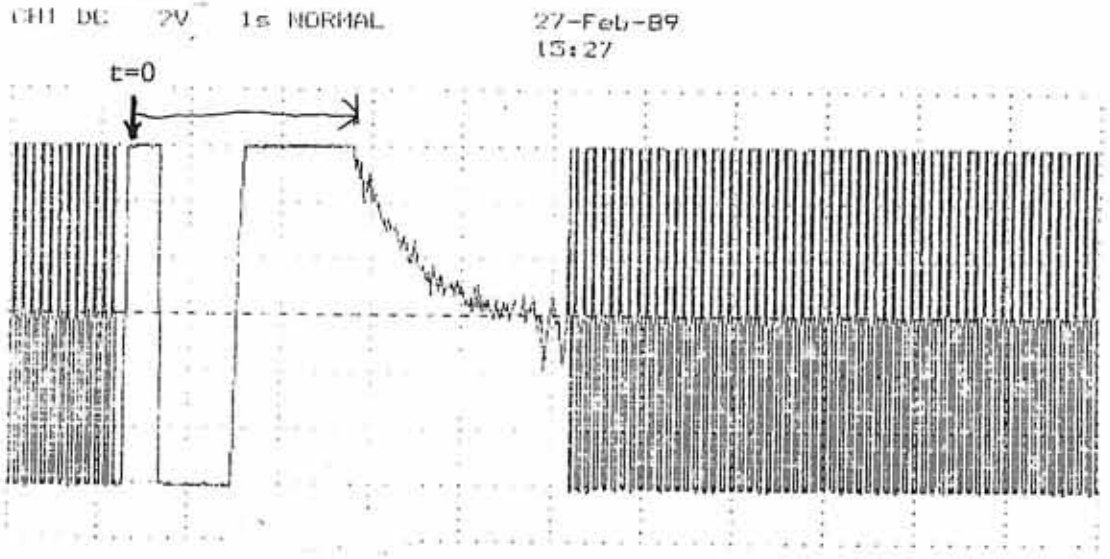
CH1 DC 2V 1s NORMAL
27-Feb-89
15:27
t=0

(a)

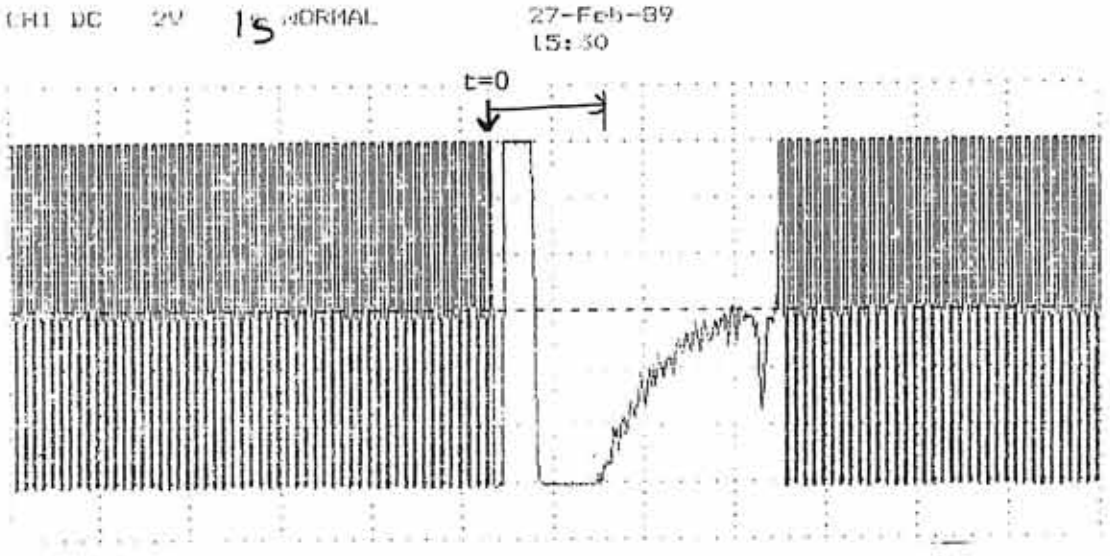
CH1 DC 2V 1s NORMAL
27-Feb-89
15:30
t=0

(b)

Figure 23. SFR-1 compressor amplifier chain output following removal of input at t=0. Input level -40 dB ref 1 V rms.

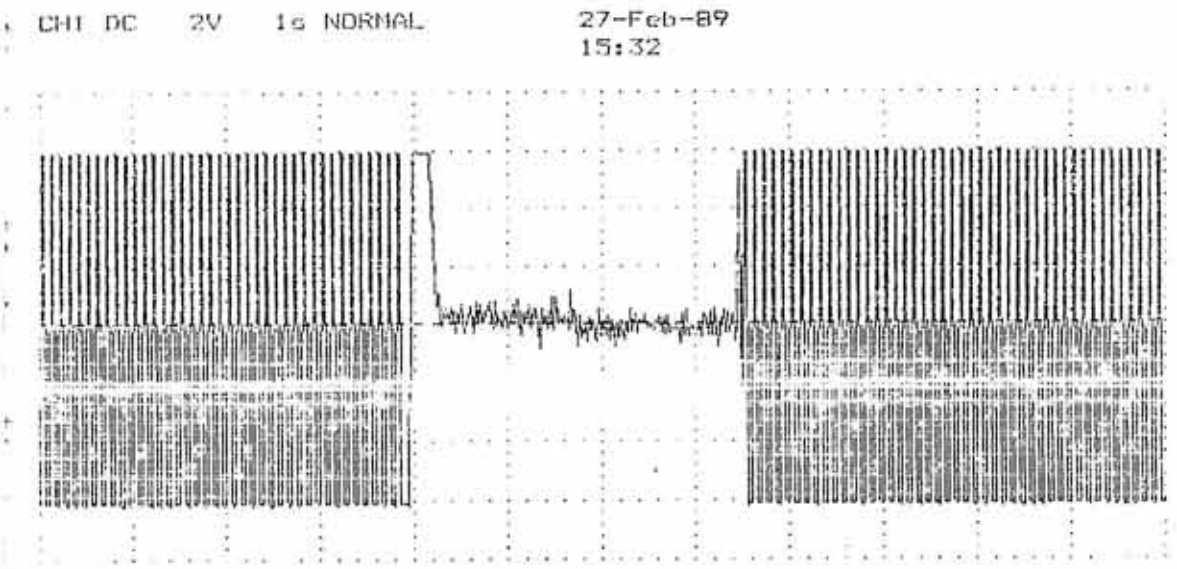
CH1 DC 2V 1s NORMAL
27-Feb-89
15:32

Figure 24. Phase response test setup of SFR-1 compressor amplifier chain, 3.3 uF coupling capacitors and 10 Hz stimulus frequency.

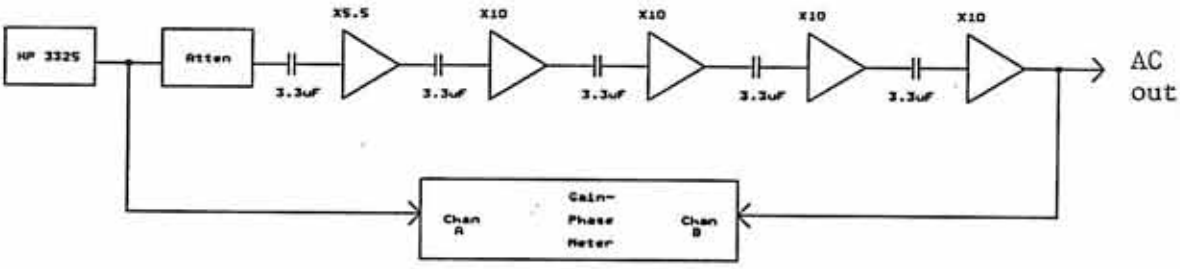
HP 3325
Atten
3.3uF
X5.5
X10
3.3uF
X10
3.3uF
X10
3.3uF
X10
3.3uF
AC
out
Chan
A
Gain-
Phase
Meter
Chan
B

Table 2. Phase Response of SFR-1 Compressor Amplifier Chain with 3.3 uF Coupling Capacitors and 10 Hz Stimulus Frequency

Attenuation(ref. 1 V rms)	Phase shift (Degrees)
0	28.0
-10	28.9
-20	30.7
-30	31.7
-40	33.7
-50	34.8
-60	37.0
-70	38.7
-80	42.6
-90	47.5

Table 3. Phase Response of SFR-3 Compressor Amplifier Chain with .45 uF Coupling Capacitors and 90 Hz Stimulus Frequency

Attenuation(ref. 1 V rms)	Phase shift (Degrees)
0	5.3
-10	6.1
-20	7.6
-30	8.3
-40	9.6
-50	10.3
-60	12.0
-70	13.5
-80	16.6
-90	21.3

the 280 ms sample interval except for the 0-dB below 1-V rms input and that the level dependent phase shift is less then that for SFR-1.

Figure 25. SFR-3 compressor with .45 uF coupling capacitors. (a) Removal of 1 V-rms, 90 Hz input. (b) Removal of .1 V-rms, 90 Hz input.

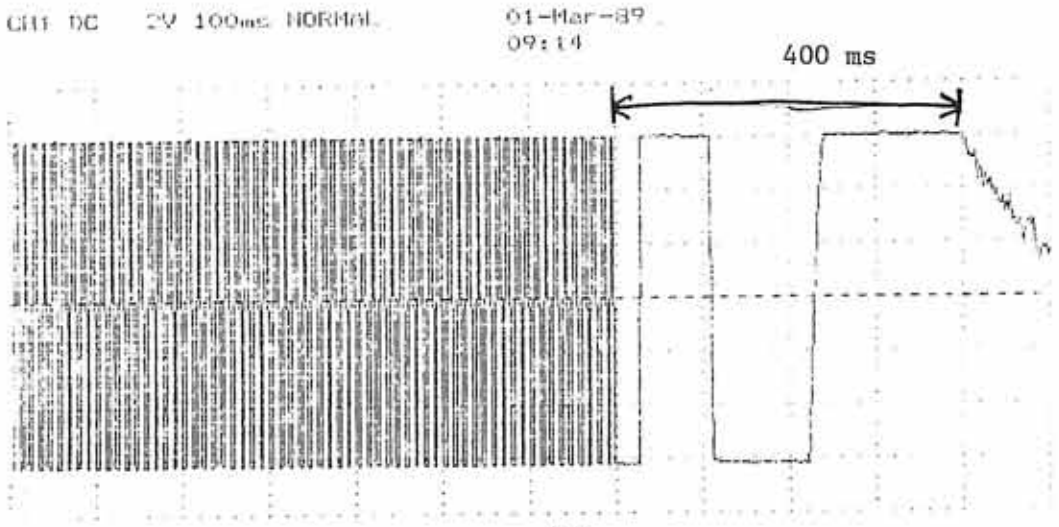
CH1 DC 2V 100ms NORMAL
01-Mar-89
09:14
400 ms

(a)

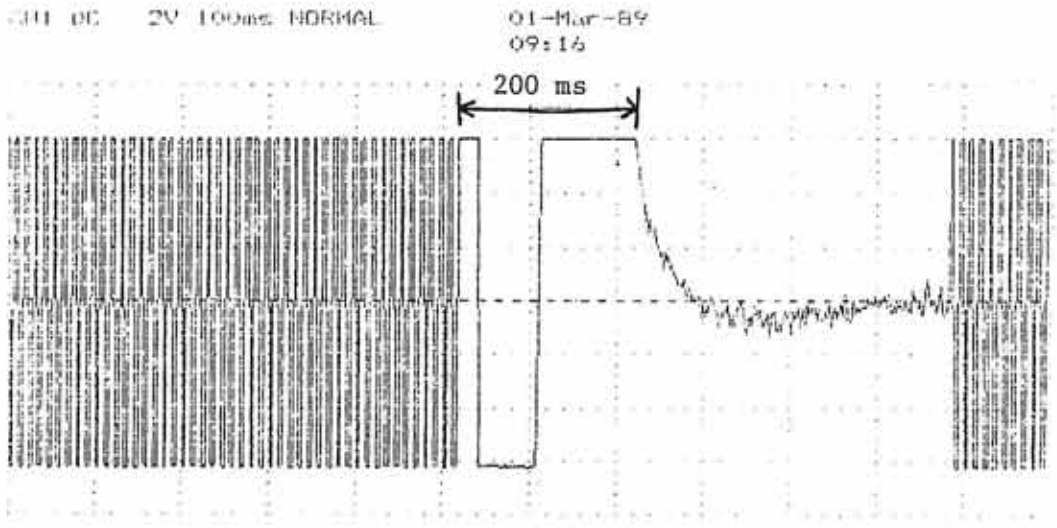
CH1 DC 2V 100ms NORMAL
01-Mar-89
09:16
200 ms

(b)

Figure 26. SFR-3 compressor with .45 uF coupling capacitors. Removal of -40 dB ref. 1 V rms input at 90 Hz.

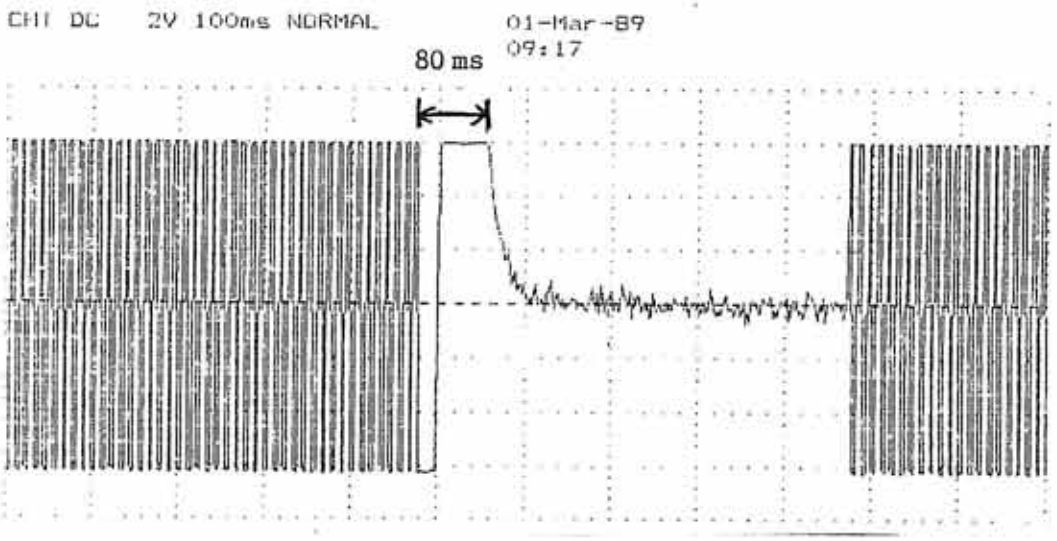
CH1 DC 2V 100ms NORMAL
01-Mar-89
09:17
80 ms

PRESENTATION AND ANALYSIS OF TEST DATA

Overview

The four major areas of receiver testing are sensitivity as a function of frequency, logarithmically compressed DC output as a function of input level, phase offset between channels, and response time of the amplitude and phase outputs to a change in the input stimulus. The frequency response plots are performed by connecting a sinusoidal stimulus and sweeping it over a wide range of logarithmically spaced frequencies for the two decade wide plots and a small range of linearly spaced frequencies for the narrow range plots. The compressed DC output verses frequency is noted and in general, for the wide range plots it is desirable that all spurious responses be at least forty decibels below the amplitude at the detection frequency. The narrow range plots show the amplitude behavior near the detection frequency, and lower sideband rejection is readily observable here.

The output verses input amplitude test is performed by applying a sinusoidal input of one volt rms through a two decibel per step attenuator at the detection frequency of the receiver. As the voltage is attenuated below the maximum input, the compressed DC output voltage is observed and a plot is constructed with the input in decibels on the horizontal axis and the DC output in volts on the

vertical axis. This graph conveniently shows compression and overload at the top of the dynamic range and the noise floor at the bottom.

The phase offset tests are performed by connecting an identical input stimulus to channels A and B. This may be either a white noise or a swept sinusoidal stimulus. The sinusoidal input is swept over the detection bandwidth of the receiver and the phase offset between channels is noted. In the ideal case, the offset would be zero but in practice a phase offset between channels due to component mismatches exists and it shows a temperature dependence.

Since many of the signals investigated by the receiver are better modeled by broadband noise instead of discrete spectra, the white noise method of phase testing provides a realistic measure of phase offset performance. A broadband white noise generator is connected to both inputs of the receiver. The phase outputs are correlated over a time interval and a phase reading weighted in accordance to the relative sensitivity verses frequency over the receiver passband results.

The response time plots are a measure of the receivers' reaction time to transient inputs. A sinusoidal input stimulus is either applied or removed. The compressed amplitude DC output rise times and fall times are noted. The hard limited AC outputs are also observed and the time interval between the application of the input and the stabilization of the phase outputs is used to determine the

time after the start of a frequency step the phase correlation may begin.

Frequency Responses

Figures 27 through 30 show the amplitude verses frequency response plots over a two decade frequency range. Figure 27 is a saturation level plot for SFR5. The first mixing frequency is held constant at 2.1 MHz and the input frequency, plotted on the horizontal axis, is swept from 50 kHz to 500 kHz. The vertical axis is the compressed DC output in volts. The sensitivity of all of the SFR channels is such that .1 volt rms at the input drives the DC output to five volts. This is approximately the maximum output for the receiver and is referred to as the saturation level output. From this plot, it is seen that the maximum output is slightly greater than five volts and the noise level is .3 volts. Since each volt at the DC output corresponds to over twenty decibels of input amplitude, this plot indicates a dynamic range of 100 decibels. Two spurious responses are evident at 300 kHz and 500 kHz. Both are more then two volts less then the five volts at 100 kHz which translates to a forty decibel spurious free response.

Figure 28 is the same as Figure 27 with the exception of a twenty decibel reduction in input level. Here the spurious responses are nearly fifty decibels down.

Figure 29 is a saturation level frequency response plot for SFR1. The first mixing frequency is held constant at 577 Hz. A 100

Figure 27. SFR-5 frequency response. -20 dB ref. 1 V rms input.

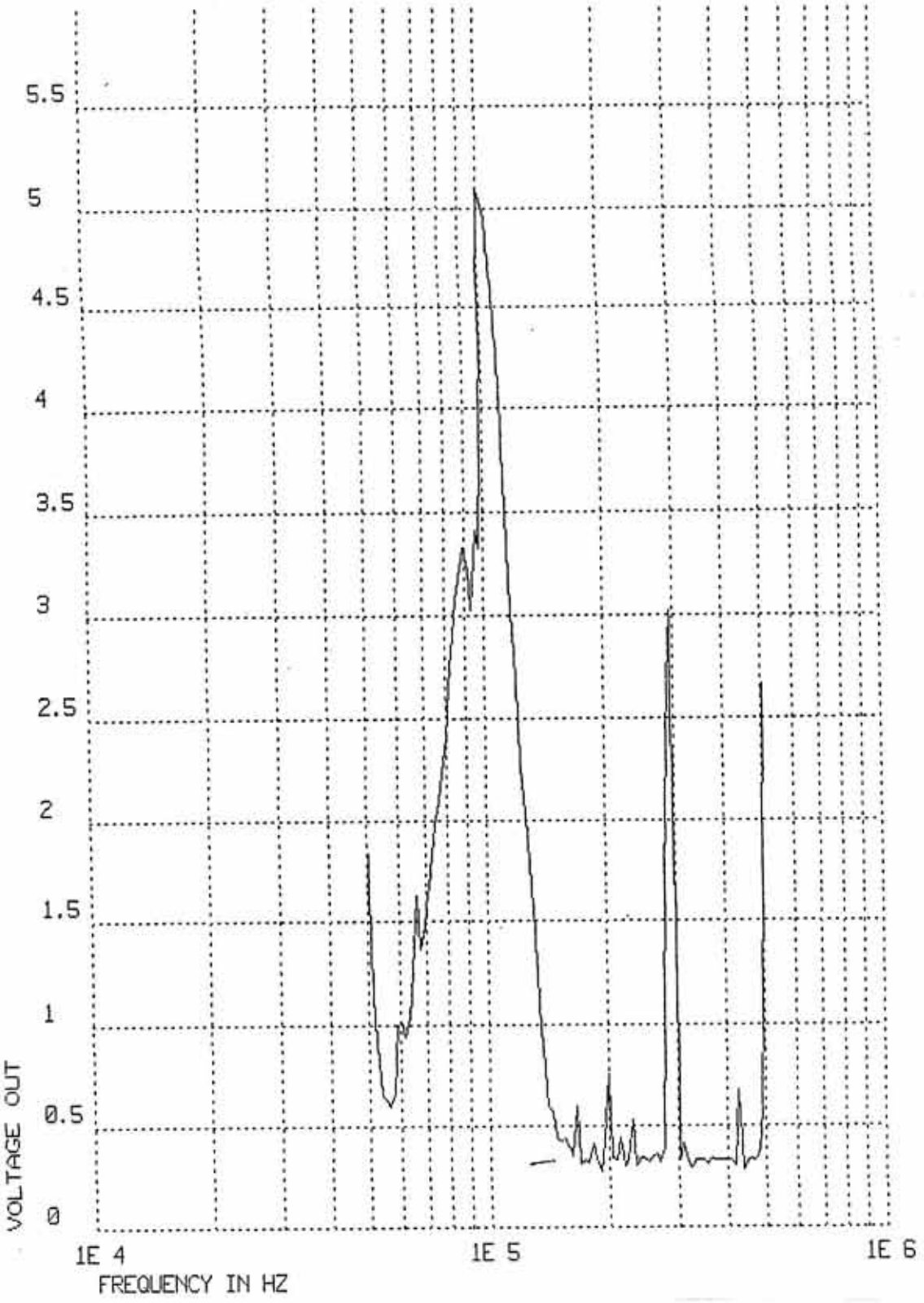
5.5
5
4.5
4
3.5
3
2.5
2
1.5
1
0.5
0
VOLTAGE OUT
1E 4
1E 5
1E 6
FREQUENCY IN HZ

Figure 28. SFR-5 frequency response. -40 dB ref. 1 V rms input.

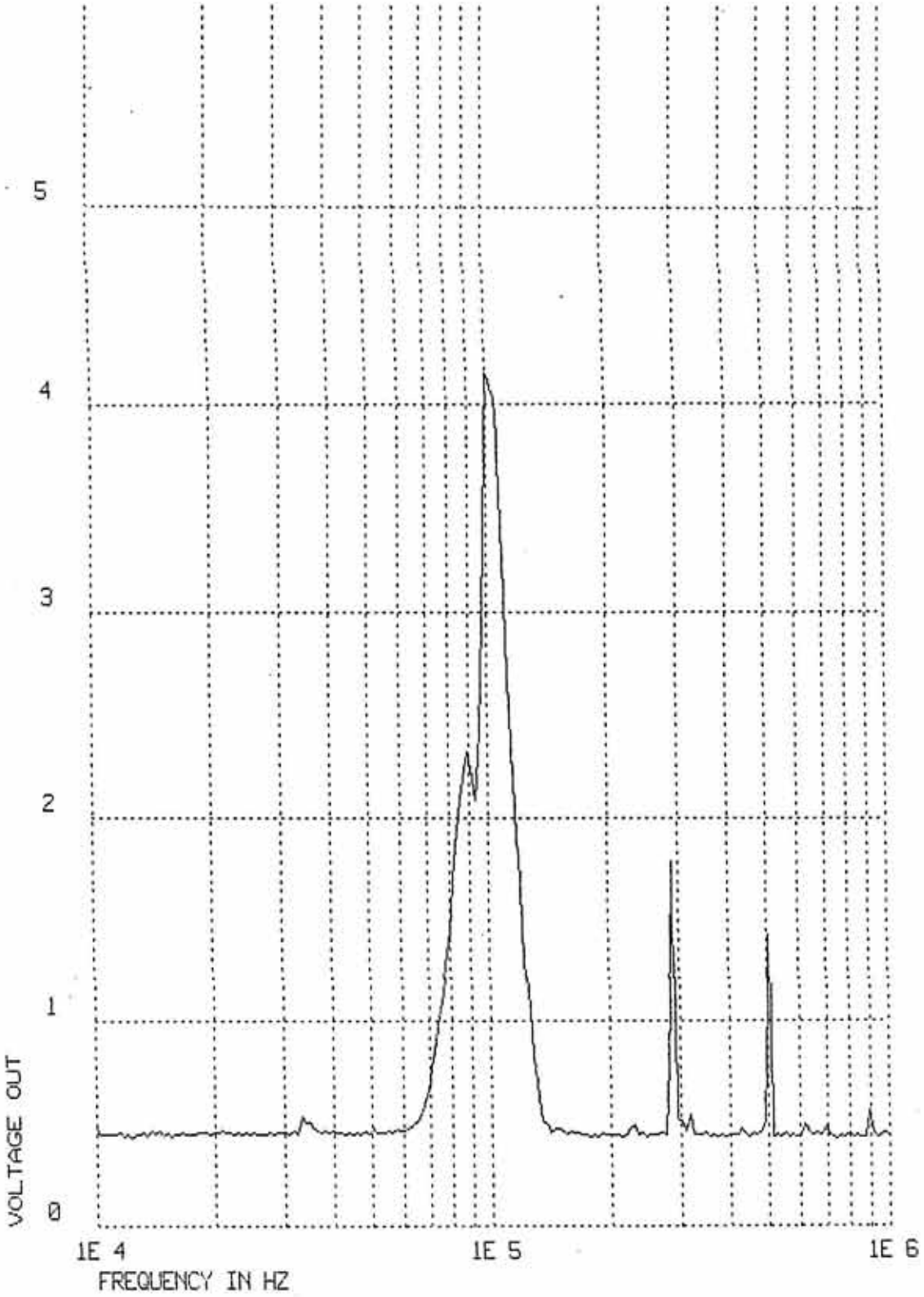
5
4
3
2
1
0
VOLTAGE OUT
1E 4
1E 5
1E 6
FREQUENCY IN HZ

Figure 29. SFR-1 frequency response. -20 dB ref. 1 V rms input.

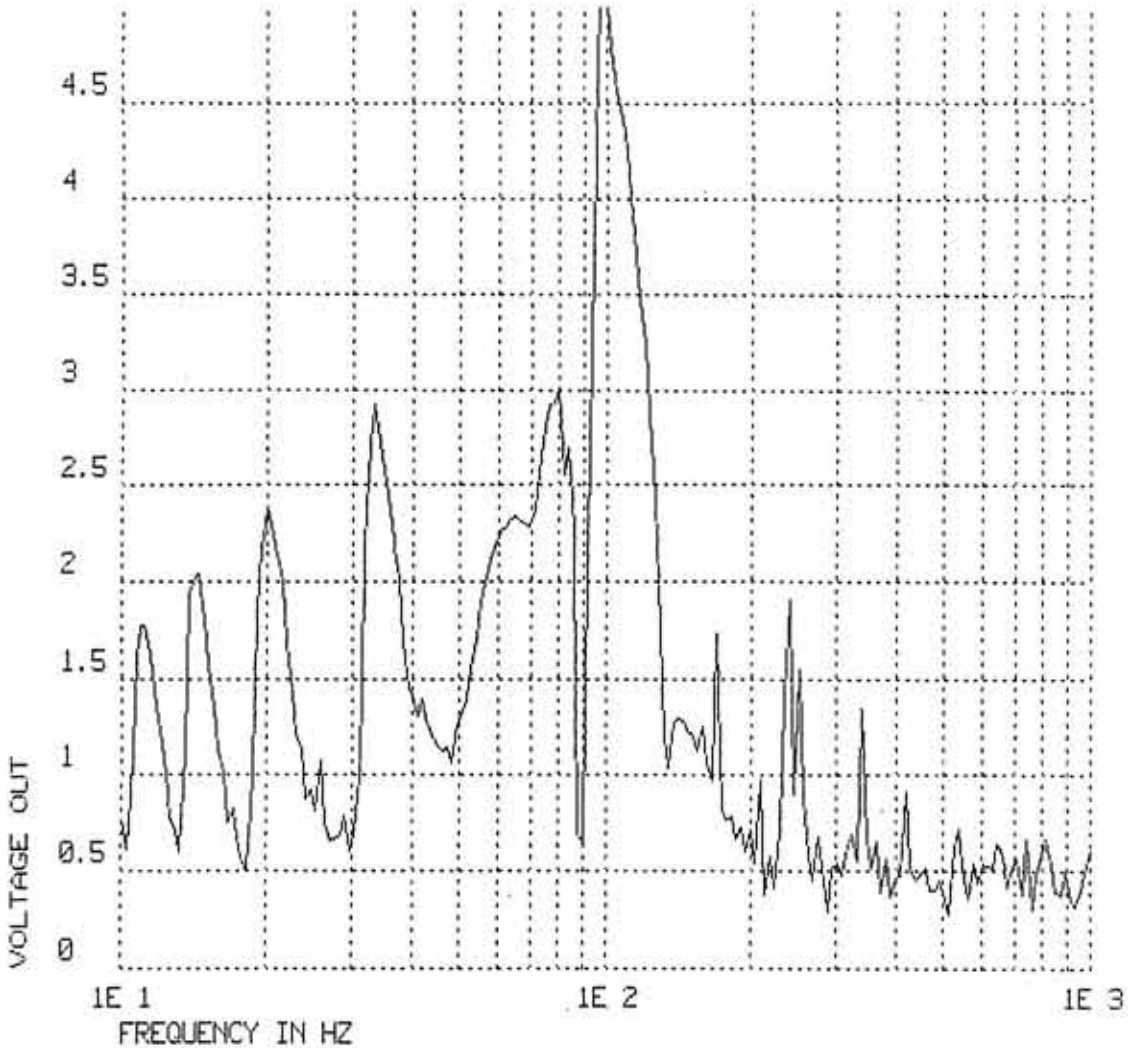
4.5
4
3.5
3
2.5
2
1.5
1
0.5
0
VOLTAGE OUT
1E 1
1E 2
1E 3
FREQUENCY IN HZ

Figure 30. SFR-1 frequency response. -40 dB ref. 1 V rms input.

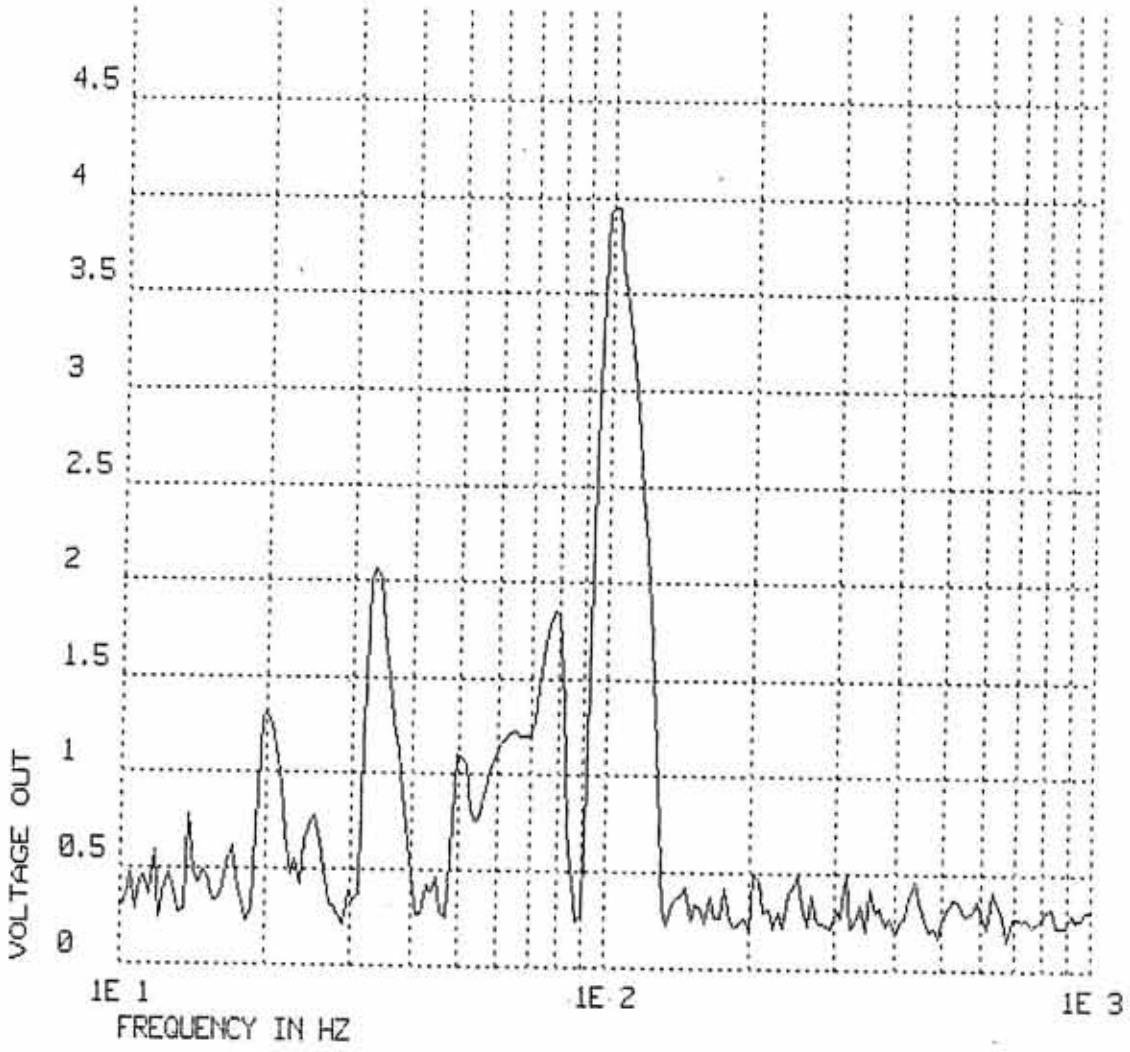
4.5
4
3.5
3
2.5
2
1.5
1
0.5
0
VOLTAGE OUT
1E 1
1E 2
1E 3
FREQUENCY IN HZ

decibel dynamic range as well as a forty decibel spurious free response is again evident. The responses between 10 Hz and 50 Hz are due to harmonic distortion in the first mixer amplifier. Figure 30 is identical to Figure 29 except for a twenty decibel reduction in input level.

Figures 31 and 32 illustrate narrow bandwidth frequency response plots for SFR5. The first mixing frequency is held constant at 2716 kHz and the input stimulus frequency is swept over a 40 kHz range to show the upper and lower sidebands. These plots show the shape of the passband and the lower sideband rejection. In both the saturation level plot (Figure 31) and in the 20 dB below saturation level plot (Figure 32) the lower sideband rejection is 40 dB. As previously mentioned, this amount of rejection is due mainly to the deviation from ninety degrees phase shift in the phase shifters.

Amplitude Responses

Figure 33 illustrates a two decibel amplitude calibration of SFR3 which clearly shows its dynamic range. It is measured by holding the stimulus frequency constant and observing the compressed DC output level while the first mixer steps through step 31. The stimulus frequency is set to the center of the detection band for step 31. The amplitude of the input is decreased in 2 dB increments from 0 to -120 dB referenced to 1 V-rms. The saturation level is -15 dB which corresponds to an output of 5.1 V. The noise floor is at

Figure 31. SFR-5 narrowband frequency response. Input level .1 V rms.

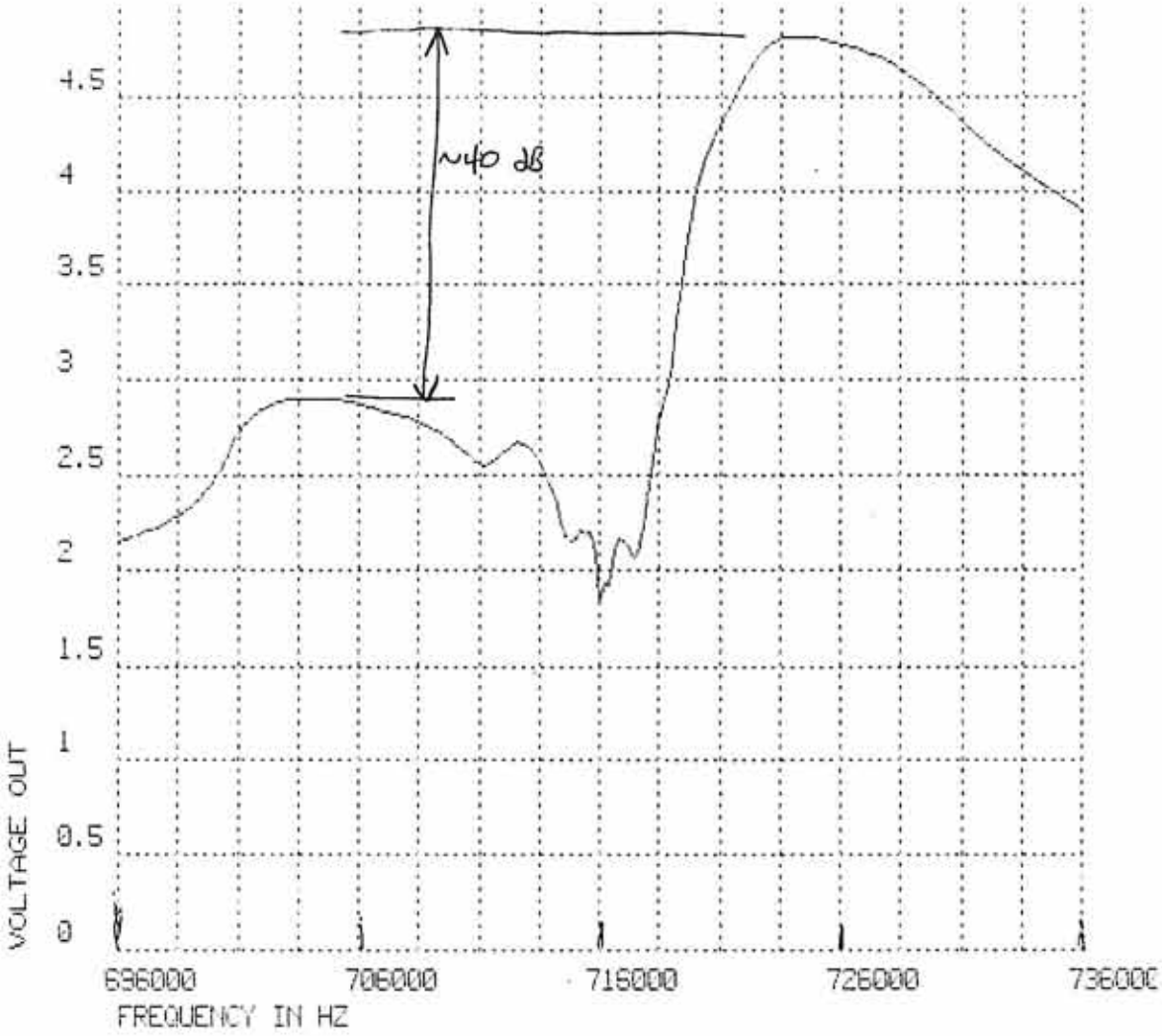
~40 dB
4.5
4
3.5
3
2.5
2
1.5
1
0.5
0
VOLTAGE OUT
696000
706000
716000
726000
736000
FREQUENCY IN HZ

Figure 32. SFR-5 narrowband frequency response. Input level .012 V rms.

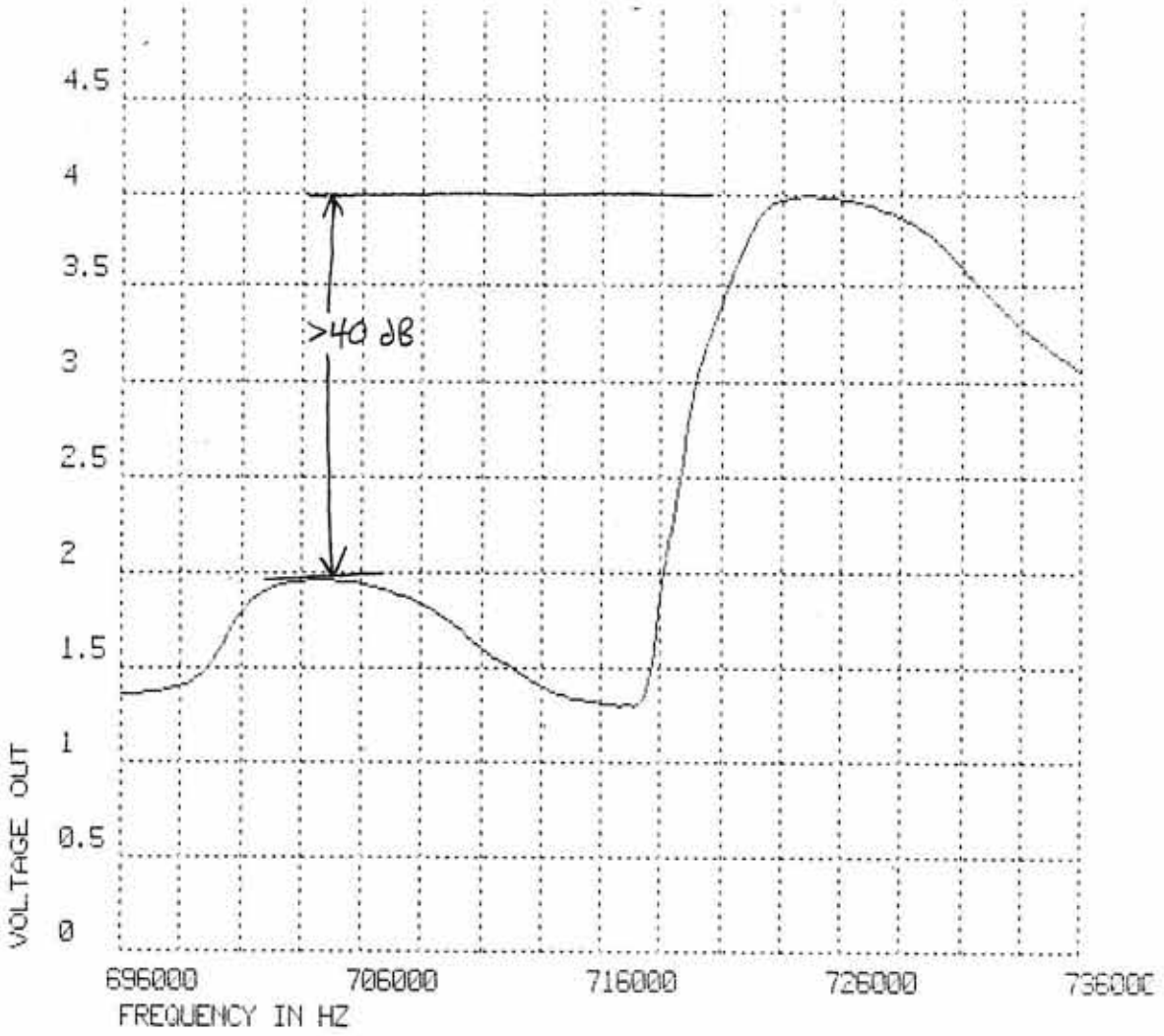
4.5
4
3.5
3
2.5
2
1.5
1
0.5
0
VOLTAGE OUT
>40 dB
696000
706000
716000
726000
736000
FREQUENCY IN HZ

Figure 33. SFR-3, step 31, 2-dB amplitude calibration. Input frequency: 12,622 Hz. Two sample average.

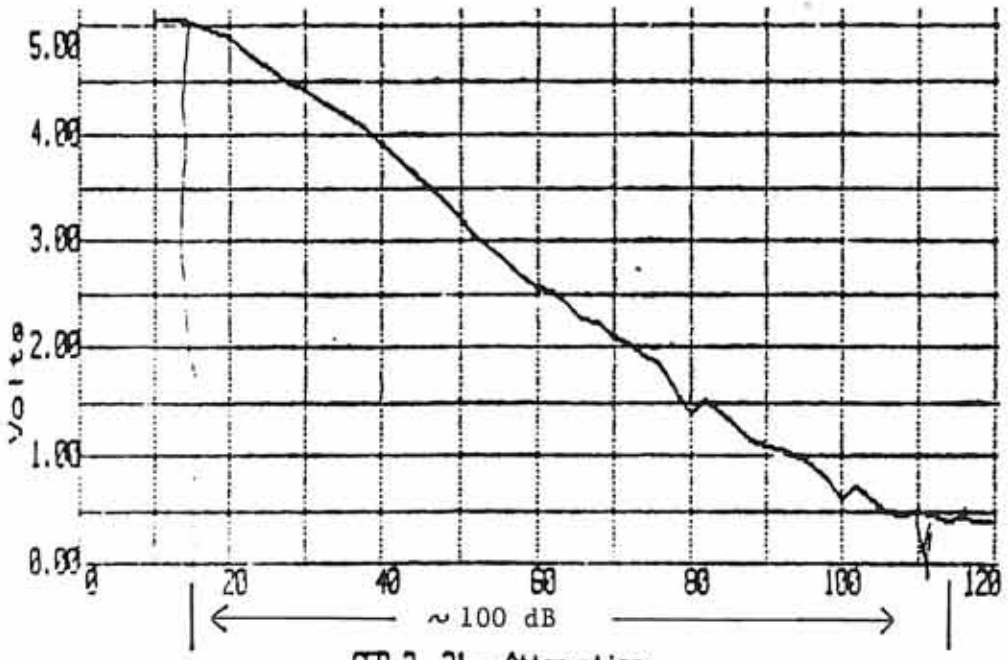

SFR 3, 31 - Attenuation

about -115 dB with an output of .4 V. this gives a dynamic range of 100 dB.

Phase Responses

In order to perform phase measurements, it is necessary that the receiver contribute minimal interchannel phase error. As mentioned, there are two ways to measure phase offset. The first is to hold the mixing frequencies constant, apply a sinusoidal excitation, and sweep the frequency over the passband. The other method is to apply noise to the inputs and observe the correlated phase angle appearing at the output. Figures 34 and 35 are examples of the former method for SFR-1. Observe that the average phase deviation over the passband shown is less than a few degrees. An example of the noise method of phase testing is shown in Table 4. Here, the 3 steps from each of the bottom three channels are shown at -40 C, +70 C, and room temperature. While there is an offset associated with each channel and step, it is reasonably minimal and is easy to calibrate out in software. Also, it has been shown that for any given temperature and amplitude level, the offset is repeatable as long as the receiver has undergone a number of hot and cold temperature conditioning cycles. This is important so that the components in the filters which influence phase shift have an opportunity to age and rid themselves of minor structural stresses. This is especially true for tantalum capacitors.

Figure 34. SFR-1 phase response over passband. Input .1 V rms.

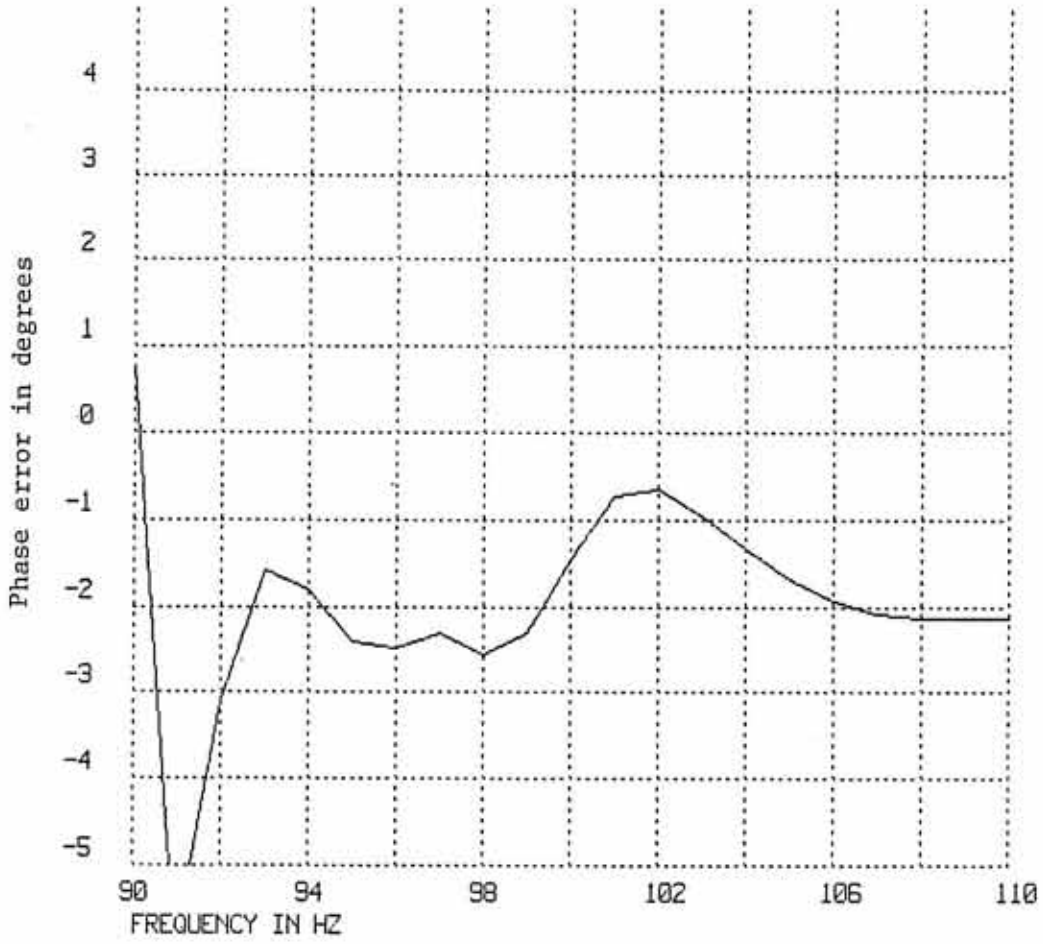
Phase error in degrees
4
3
2
1
0
-1
-2
-3
-4
-5
90
94
98
102
106
110
FREQUENCY IN HZ

Figure 35. SFR-1 phase response over passband. Input .01 V rms.

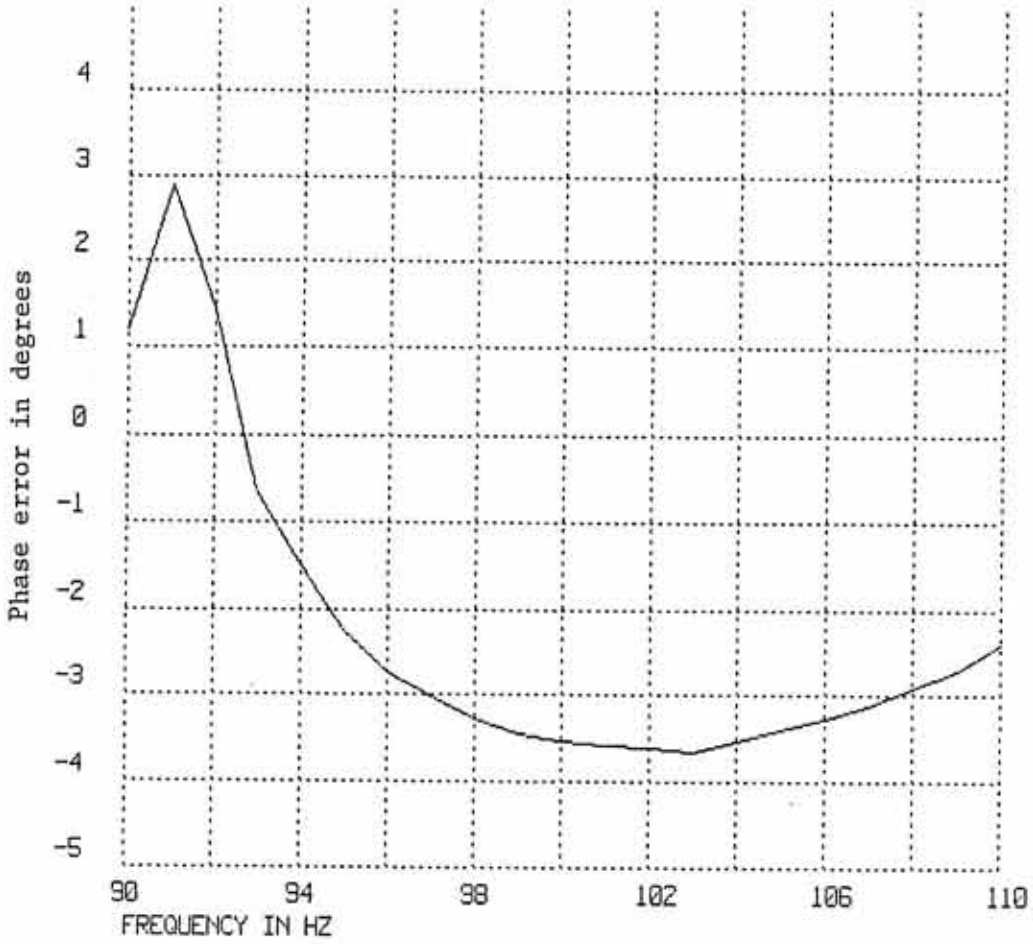
Phase error in degrees
4
3
2
1
0
-1
-2
-3
-4
-5
90
94
98
102
106
110
FREQUENCY IN HZ

Table 4. White Noise Phase Numbers

SFR/Step	Phase (degrees) Room temp	-40 C	+70 C
1-1	10.4	9.5	11.5
1-15	12.4	11.3	11.9
1-31	12.1	8.7	17.8
2-1	-2.6	16.9	-10.5
2-15	-5.5	16.8	-3.7
2-31	-9.1	15.0	-.4
3-1	-3.4	-8.8	-3.4
3-15	-3.4	-9.2	-4.7
3-31	-3.9	-10.1	-2.7

Time Domain Response

Although frequency selectivity and dynamic range are the primary parameters of interest in this receiver, it is important that the response time be adequate to permit the receiver to respond within the time interval it spends on a step. Figures 36 and 37 show the application and removal respectively of saturation level inputs to SFR-3. Note that the response is complete well before the 280 ms step interval which indicates that a sample of the DC level may be accurately be made in this time.

Determination of Phase Correlation Times

Figure 38 illustrates the test arrangement for the determination of phase correlation time test. Three independent white noise generators are connected through an arrangement of attenuators to a

Figure 36. SFR-3, step 27 compressor DC output. T=0: application of .1 V rms, 8883 Hz input.

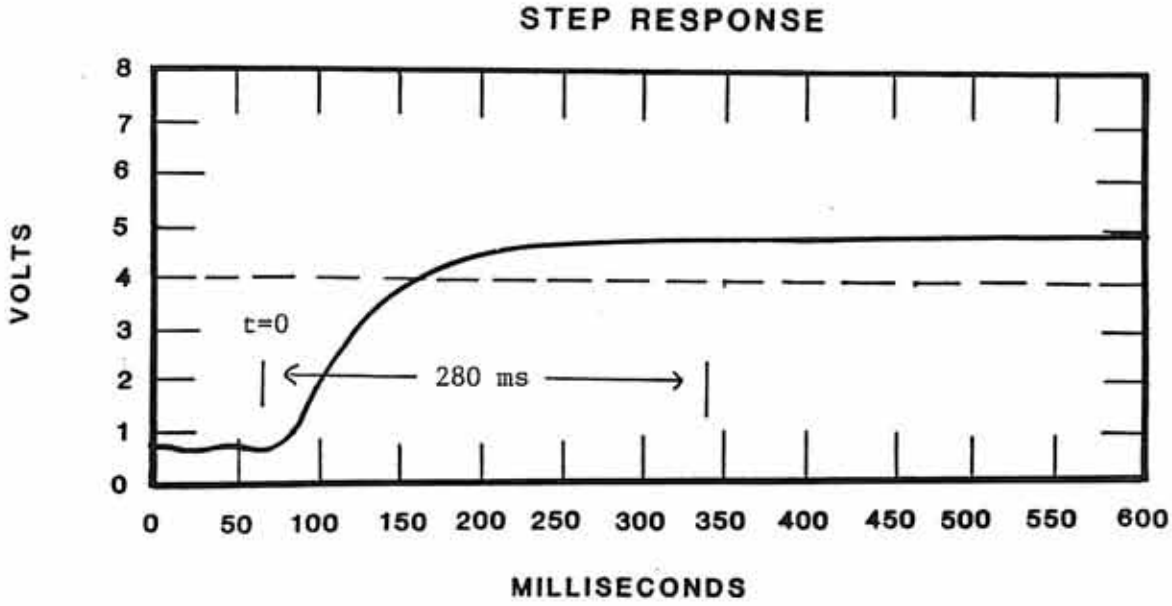
STEP RESPONSE
VOLTS
8
7
6
5
4
3
2
1
0
t=0
280 ms
0
50
100
150
200
250
300
350
400
450
500
550
600
MILLISECONDS

Figure 37. SFR-3, step 27 compressor DC output. T=0: removal of .1 V rms, 8883 Hz input.

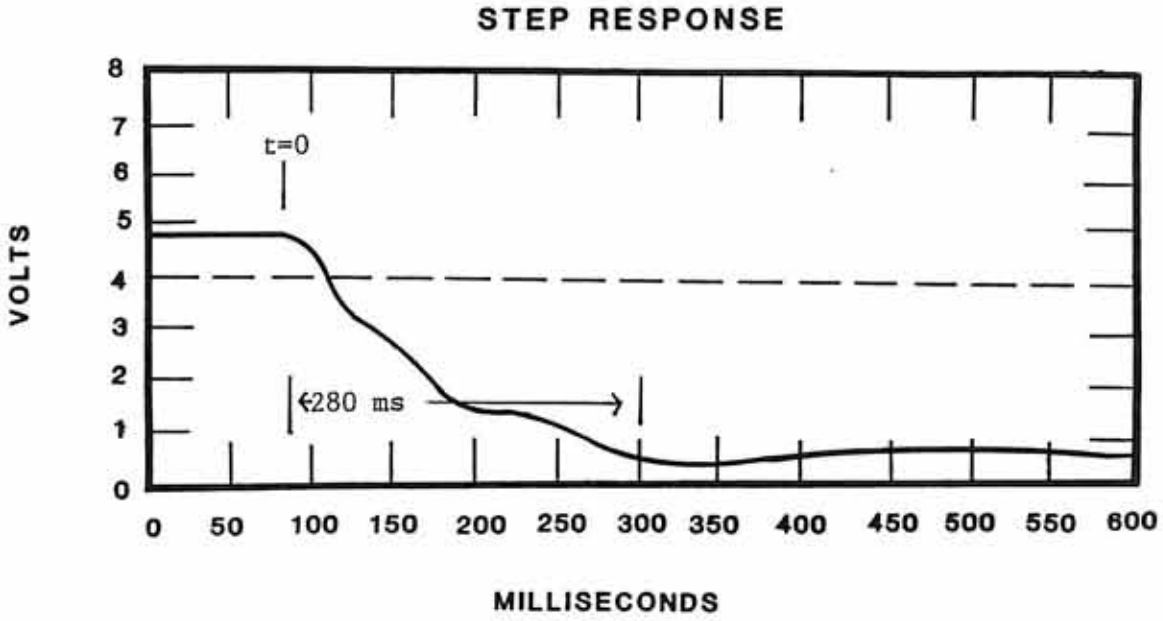
STEP RESPONSE
VOLTS
8
7
6
5
4
3
2
1
0
t=0
←280 ms
0
50
100
150
200
250
300
350
400
450
500
550
600
MILLISECONDS

Figure 38. Test setup for average correlation vs. standard deviation of phase test

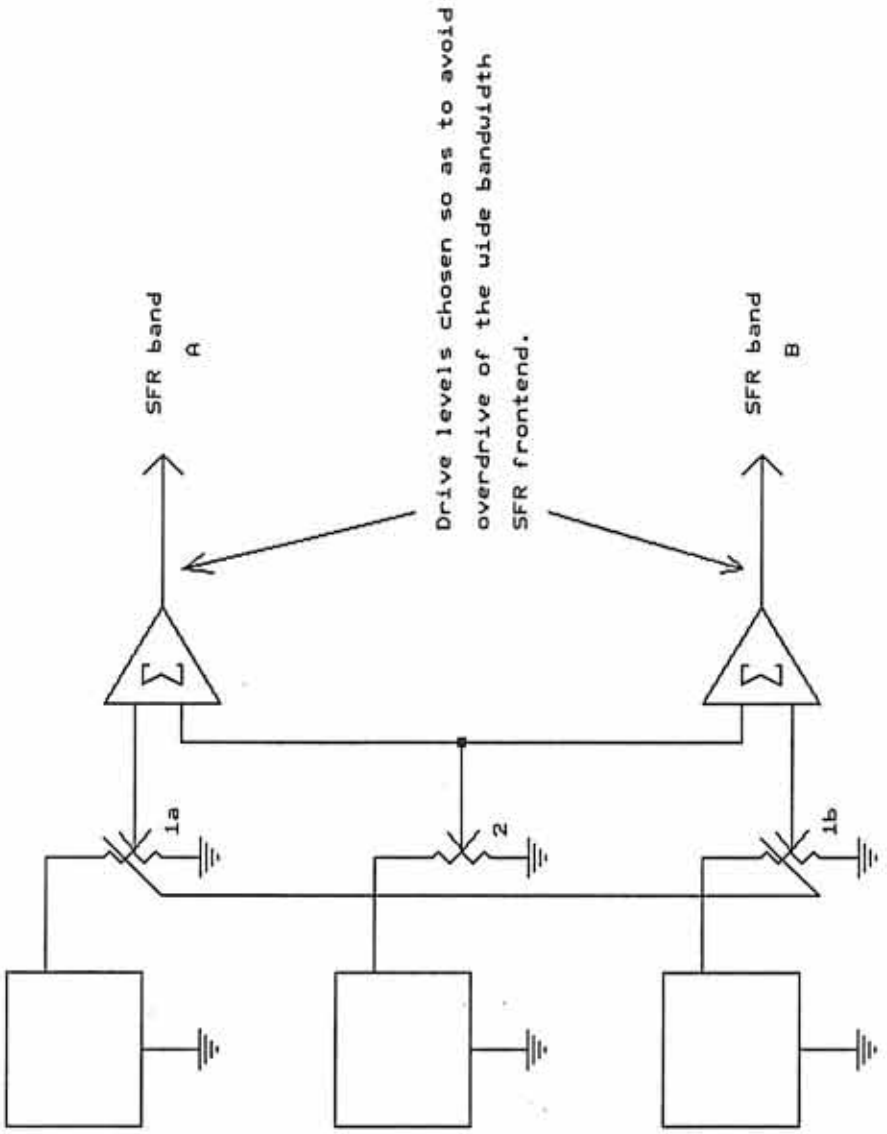
SFR band
A
Drive levels chosen so as to avoid
overdrive of the wide bandwidth
SFR frontend.
SFR band
B
1a
2
1b
General Radio Gaussian
White Noise Generators

pair of summing amplifiers. These are connected to the two inputs of the receiver. The front-end stages of the receiver are monitored throughout the test to insure that over driving does not occur. The bandwidth is widest at the front of the receiver and saturation is possible with wide bandwidth signals such as white noise. Table 5 is a tabulation of standard deviation and correlation for an integration time of .10 seconds for SFR3. The level of the white noise generator which drives both channels is varied relative to those that only drive a single channel. In this way it is possible to vary the correlation between the noise stimuli between the two channels. The standard deviation of the phase between channels and the correlation is calculated. Figure 39 illustrates the average correlation versus standard deviation of phase for five integration times for SFR3. It is observed that the relation between correlation and standard deviation changes little for integration times greater than .25 seconds. The final integration time for SFR3 is determined by several additional system timing constraints and is .22 seconds. The detection bandwidths and integration times for all of the bands are summarized here:

SFR	1	2	3	4	5
Detection Bandwidth	5 Hz	15.6 Hz	125 Hz	1.0 kHz	8.0 kHz
Integration Time	.51s	.44s	.22s	31ms	31ms

Table 5. Determination of Standard Deviation and Correlation for an Integration Time of .10 s for SFR-3

Integration Time 5161 (0.10 sec)
Number of Data Points: 100
Attenuator Step Size: 1
Attenuator Start Value: -20

Attenuator	Sin		Cos		Correlation		Phase	
Value	Avg.	SD	Avg.	SD	Avg.	SD	Avg.	SD
-20	10453	425	1105	282	0.987	0.008	0.323	3.704
-19	10442	427	1160	323	0.986	0.009	0.235	3.741
-18	10399	448	1261	362	0.983	0.011	-0.139	3.938
-17	10428	453	1374	373	0.979	0.012	0.118	3.993
-16	10414	414	1518	406	0.974	0.016	-0.003	3.665
-15	10365	509	1763	477	0.965	0.022	-0.449	4.553
-14	10413	653	2166	533	0.949	0.025	0.028	6.031
-13	10475	617	2203	533	0.947	0.027	0.552	5.629
-12	10446	695	2722	606	0.919	0.035	0.302	6.662
-11	10454	736	3019	775	0.899	0.053	0.361	7.096
-10	10451	810	3342	739	0.879	0.055	0.410	7.995
-9	10402	857	3539	810	0.864	0.064	-0.016	8.665
-8	10341	904	3898	942	0.835	0.083	-0.659	9.258
-7	10541	919	4198	878	0.811	0.078	1.534	9.783
-6	10473	1024	4552	971	0.780	0.094	0.642	11.321
-5	10417	1133	5172	1048	0.722	0.111	0.215	13.771
-4	10483	1139	5396	1092	0.700	0.119	1.992	15.313
-3	10747	1229	5954	1187	0.643	0.135	4.978	17.266
-2	10319	971	6314	1228	0.590	0.143	-1.384	16.180
-1	10503	1075	6567	1056	0.566	0.125	1.479	17.599
0	10591	1203	7180	1259	0.496	0.159	1.683	24.266
1	10462	1394	7942	1067	0.415	0.143	2.186	31.435
2	10437	1251	8191	1391	0.391	0.153	3.020	43.810
3	10342	1451	8474	1315	0.364	0.166	5.237	49.289
4	10409	1274	8879	1396	0.322	0.149	-2.833	59.484
5	10619	1234	8990	1281	0.303	0.144	7.410	59.997
6	10474	1246	9349	1569	0.295	0.152	-3.550	75.923
7	10606	1398	9807	1427	0.273	0.142	10.354	87.280
8	10421	1518	9598	1255	0.281	0.139	6.284	78.984
9	10157	1420	9825	1319	0.262	0.145	-7.749	86.673
10	10495	1325	9856	1243	0.250	0.126	6.179	86.774
11	10644	1220	10003	1385	0.249	0.130	22.550	86.322
12	10369	1162	9950	1393	0.241	0.134	3.787	94.271
13	10577	1306	10242	1294	0.243	0.124	13.734	96.803
14	10476	1320	10021	1262	0.252	0.112	5.804	92.442
15	10389	1386	10025	1228	0.246	0.131	8.893	96.191
120	10649	1338	10397	1218	0.245	0.112	16.662	100.998

Figure 39. Graph of correlation verses standard deviations for five integration times.

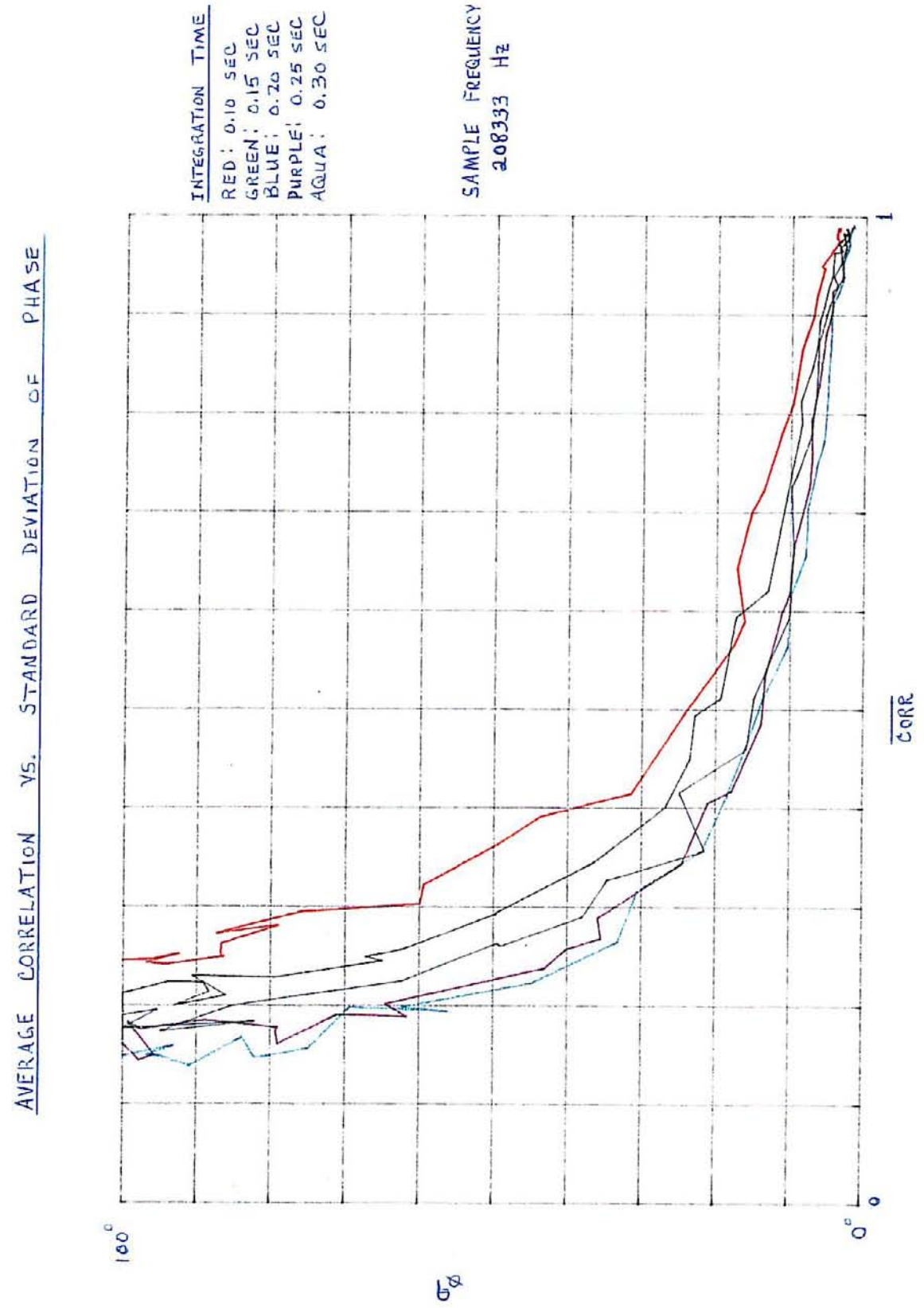
AVERAGE CORRELATION VS. STANDARD DEVIATION OF PHASE
INTEGRATION TIME
RED: 0.10 SEC
GREEN: 0.15 SEC
BLUE: 0.20 SEC
PURPLE: 0.25 SEC
AQUA: 0.30 SEC
SAMPLE FREQUENCY
208333 Hz
100°
0°
σφ
0
1
CORR

Figure 40 shows the outputs of the sine and cosine counters as a function of the phase angle between the receiver inputs for a sinusoidal excitation at the center of the detection band. The plot shows a linear relationship between the counts and phase.

Figure 40. Output of sine and cosine counters as a function of phase angle between the receiver inputs for a sinusidal exitation

46 0410

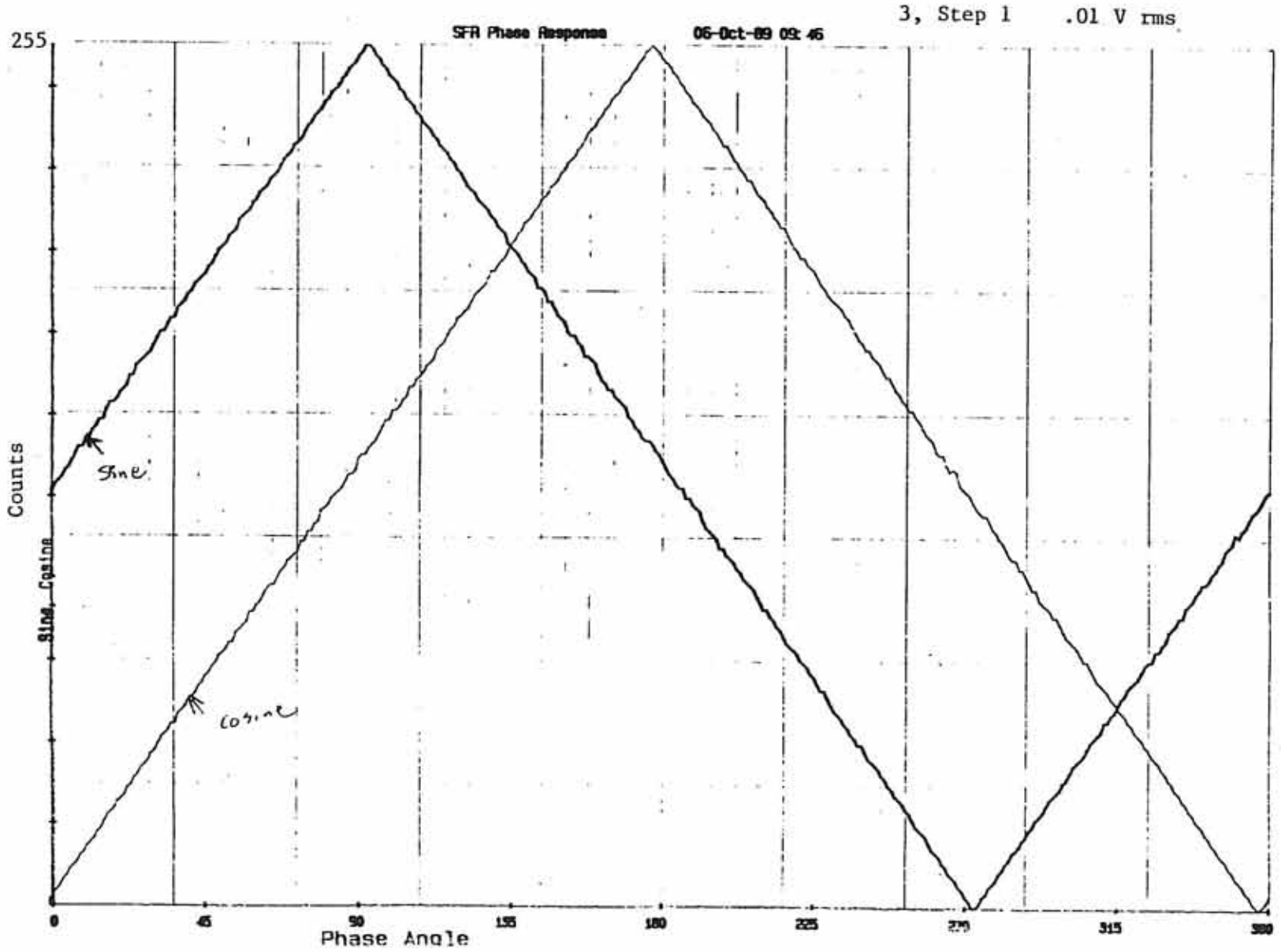
3, Step 1 .01 V rms
SFR Phase Response
06-Oct-89 09:46
255
Counts
Sine, Cosine
Sine
Cosine
0
45
90
135
180
225
270
315
360
Phase Angle

CONCLUSIONS

The methods and instrumentation described in this thesis have shown that it is possible to construct a receiver that provides measurements of signals detected by a system of antennas mounted to a spacecraft that exceeds previous levels of performance. These include both amplitude and phase measurements of electromagnetic and electrostatic stimuli. Because of the wide dynamic range amplitude and high resolution phase capabilities, it is possible to observe many characteristics of electrostatic and electromagnetic waves.

LIST OF REFERENCES

1. Calvert, W., 1985: "DE-1 Measurements of AKR Wave Directions," Geophysical Research Letters, Vol. 12, No. 6, pp. 381-384, June 1985.

2. Chen, H., 1974: "Dynamic Source Structure of Type III Solar Radio Bursts at 26.4 MHz" Thesis, University of Iowa, p.1, pp. 132-136.

3. Weaver, Donald K., 1953: "Design of RC Wide-Band 90-Degree Phase Difference Network," Proceedings of the I.R.E., pp. 671-676.

APPENDIX 1. MATHEMATICAL DERIVATION OF SINGLE SIDEBAND CONVERSION METHOD

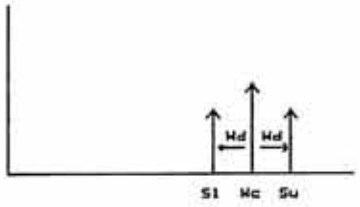

Let $x(t) = S_\ell(t)e^{j(\omega_c-\omega_\partial)t} + S_u(t)e^{j(\omega_c+\omega_\partial)t}$, $S_\ell(t) = S_u(t)$

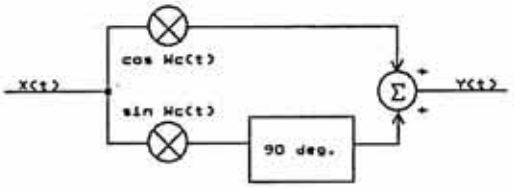

$$x(t)\cos\omega_c(t) = \frac{1}{2}S_\ell(t)\left[e^{j(\omega_c-\omega_\partial)t}\left(e^{j\omega_c t} + e^{-j\omega_c t}\right)\right]$$

$$+ \frac{1}{2}S_u(t)\left[e^{j(\omega_c+\omega_\partial)t}\left(e^{j\omega_c t} + e^{-j\omega_c t}\right)\right]$$

$$= \frac{1}{2}S_\ell(t)\left[e^{j(2\omega_c-\omega_\partial)t} + e^{-j\omega_\partial t}\right] + \frac{1}{2}S_u(t)\left[e^{j(2\omega_c+\omega_\partial)t} + e^{j\omega_\partial t}\right]$$

Filter baseband and eliminate $2\omega_c$ terms

$$= \frac{1}{2} S_\ell(t)\, e^{-j\omega_\partial t} + \frac{1}{2} S_u(t) e^{j\omega_\partial(t)}$$

Similarly,

$$x(t) \sin \omega_c(t) = - \frac{1}{2j} S_\ell(t) e^{-j\omega_\partial(t)} - \frac{1}{2j} S_u(t) e^{j\omega_\partial t}$$

$\frac{\pi}{2}$ block in figure is represented by Hilbert transform

$$H_s(f) = \begin{cases} -j\ S(f), & f > 0 \\ +j\ S(f), & f < 0 \end{cases}$$

$$H[x(t) \sin \omega_c t] = - \frac{1}{2} S_\ell(t) e^{-j\omega_\partial t} + \frac{1}{2} S_u(t) e^{j\omega_\partial t}$$

$$Y(t) = x(t) \cos \omega_c t + H[x(t) \sin \omega_c(t)] = \boxed{S_u(t) e^{j\omega_\partial t}}$$

Upper sideband term

APPENDIX 2. RESULT OF DISTORTION IN SECOND MIXER

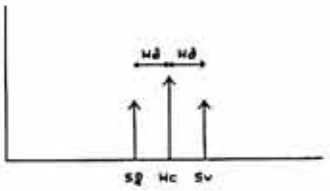

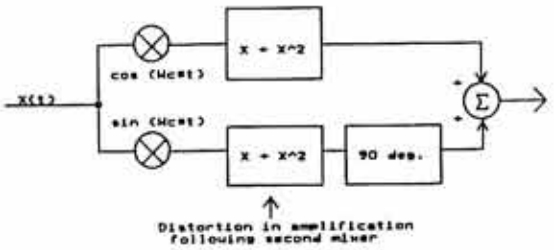

$$\cos(\omega_c t) = \frac{1}{2}\left[e^{j\omega_c t} + e^{-j\omega_c t}\right], \quad \sin(\omega_c t) = \frac{1}{2j}\left[e^{j\omega_c t} - e^{-j\omega_c t}\right]$$

$$x(t)\cos(\omega_c t) = \left[S_\ell(t)e^{j(\omega_c-\omega_\partial)t} + S_u(t)e^{j(\omega_c+\omega_\partial)t}\right]\frac{1}{2}\left[e^{j\omega_c t} + e^{-j\omega_c t}\right]$$

$$= \frac{1}{2}\left[S_\ell(t)e^{j(\omega_c-\omega_\partial)t}e^{j\omega_c t} + S_\ell(t)e^{j(\omega_c-\omega_\partial)t}e^{-j\omega_c t}\right.$$

$$\left. + S_u(t)e^{j(\omega_c+\omega_\partial)t}e^{j\omega_c t} + S_u(t)e^{j(\omega_c+\omega_\partial)t}e^{-j\omega_c t}\right]$$

Neglect $2\omega_c$ terms (Baseband filter eliminates these)

$$= \frac{1}{2}\left[S_\ell(t)\, e^{-j\omega_\partial t} + S_u(t)e^{j\omega_\partial t}\right]$$

Now, add second harmonic to this

$$= \frac{1}{2}\left[S_\ell(t)\, e^{-j\omega_\partial t} + S_u^2(t) e^{j2\omega_\partial t} + S_u(t) e^{j\omega_\partial t} + S_u^2(t) e^{j2\omega_\partial t}\right]$$

Similarly,

$$x(t) \sin(\omega_c t) = \frac{1}{j2}\left[-S_\ell(t)\, e^{-j\omega_\partial t} - S_u(t) e^{j\omega_\partial t}\right]$$

Add second harmonic:

$$= \frac{1}{j2}\left[-S_\ell(t)\, e^{-j\omega_\partial t} + S_\ell^2(t) e^{-j2\omega_\partial t} - S_u(t) e^{j\omega_\partial t} + S_u^2(t) e^{j2\omega_\partial t}\right]$$

Hilbert transform: $H_s(f) = \begin{cases} -jS(f), & f > 0 \\ +jS(f), & f < 0 \end{cases}$

$$= \frac{-S_\ell(t)}{2} e^{-j\omega_\partial t} + \frac{S_\ell^2(t)}{2} e^{-j2\omega_\partial t} + \frac{S_u(t)}{2} e^{j\omega_\partial t} - \frac{S_u^2(t)}{2} e^{j2\omega_\partial t}$$

Form sum: $\underbrace{S_u(t) e^{j\omega_\partial t}}_{\text{Desired term}} + \underbrace{S_\ell^2(t)\, e^{-j\omega_\partial t}}_{\text{Undesired lower sideband term}}$